Quark Flavor Tagging in Polarized Semi-Inclusive Deep Inelastic Scattering

by

Janusz Michael Niczyporuk

Submitted to the Department of Physics
in partial fulfillment of the requirements for the degree of

Bachelor of Science

at the

MASSACHUSETTS INSTITUTE OF TECHNOLOGY

June 1997

Author . . . .
Department of Physics
May 12, 1997

Certified by . . . .
Robert P. Redwine
Professor of Physics
Thesis Supervisor

Certified by . . . .
Richard G. Milner
Associate Professor of Physics
Thesis Supervisor

Accepted by . . . .
Professor June L. Matthews
Senior Thesis Coordinator, Department of Physics

Quark Flavor Tagging in Polarized Semi-Inclusive Deep Inelastic Scattering

by

Janusz Michael Niczyporuk

Submitted to the Department of Physics
on May 12, 1997, in partial fulfillment of the
requirements for the degree of
Bachelor of Science

Abstract

This thesis describes the theory and phenomenology of quark flavor tagging using semi-inclusive hadrons in deep inelastic scattering, with emphasis on the HERMES experiment at HERA (DESY, Hamburg, Germany). In particular, it presents a coherent treatment of the connection between partonic and hadronic degrees of freedom. As an application of these ideas, a formalism is introduced that allows one to relate quark spin distributions to the semi-inclusive asymmetries accessible at HERMES. The sensitivity of various semi-inclusive hadrons to different quark flavors is studied using the Monte Carlo simulation program PEPSI.

The only data that currently exist for semi-inclusive, spin-dependent deep inelastic scattering involve longitudinally polarized targets. In comparison to the longitudinal case, relatively little attention has been focused on physics involving transverse polarization. To further motivate the interest in semi-inclusive reactions off transversely polarized nucleons, this thesis also proposes a new method to measure the gluon contribution to the total helicity of the nucleon using a comparison of the twist-2 polarized structure functions g_1 and h_1. It is demonstrated that a measurement of h_1 is feasible at HERMES.

Thesis Supervisor: Robert P. Redwine
Title: Professor of Physics

Thesis Supervisor: Richard G. Milner
Title: Associate Professor of Physics

Acknowledgments

This thesis represents the culmination of several years of work and would not have been possible without the assistance and encouragement of many people. I would like to take this opportunity to thank them for their support throughout the years.

I owe great gratitude to my thesis advisors, Bob Redwine and Richard Milner, for providing me with the extraordinary opportunity of becoming, as an undergraduate, an active member of their research groups and, particularly, the HERMES experiment. My numerous experiences were truly invaluable and will, I am sure, influence me for many years to come, both as a physicist and as a person. I appreciate the freedom that they gave me in finding solutions to important problems in the field, together with complete responsibility for carrying out those solutions. I would also like to convey my appreciation to the Undergraduate Research Opportunities Program (UROP) at MIT, which makes experiences such as mine possible.

I would like to thank all of my colleagues within the HERMES collaboration for their contributions to this joint endeavor; I wish them many successes in the future. Several people deserve, in my mind, special mention. I would like to express my gratitude to Eppo Bruins for his unique spirit, his words of encouragement, and his friendship. Many of the key ideas in this thesis have originated from our numerous conversations at the DESY Cafeteria; working with him has been immensely rewarding. I also wish to acknowledge Roy Holt, who has been a constant source of invaluable insight and encouragement. I look forward to further stimulating discussions when I join the physics department at UIUC next fall, albeit working with the High Energy Group on the CDF experiment. A special thanks goes to Sergey Rudnitsky, whose lively conversations made the food at the DESY Bistro ever more bearable; I wish him much success in his soon to be physics-free life.

I would like to acknowledge the wisdom and insight of several theorists, especially Bob Jaffe, Xiangdong Ji, and Lech Mankiewicz, who have contributed greatly to my progress and understanding. I particularly wish to thank Xiangdong for inviting me to give a talk—my first seminar talk—at the Institute for Nuclear Theory in Seattle. I sincerely hope that I have the opportunity to interact with them in the future.

Lastly, and most importantly, I would like to thank my family for their love and encouragement. I only wish that my deceased mother, Nina, could have lived to celebrate these moments in my life.

Contents

List of Figures

List of Tables

Chapter 1

Introduction

This thesis describes the physics of spin-dependent, semi-inclusive leptoproduction of hadrons:

$$\vec{\ell}(k^\mu) \; + \; \vec{N}(P^\mu) \; \longrightarrow \; \ell'(k'^\mu) \; + \; h(h^\mu) \; + \; X \tag{1.1}$$

To lowest order in α_{em}, this process is mediated by the exchange of a spacelike virtual photon $\gamma^*(q^\mu)$ between the polarized lepton $\vec{\ell}$ and polarized target nucleon $\vec{N}$. The kinematic variables that are used to describe such an event are defined in 1.1.

In the $Q^2, \nu \rightarrow \infty$ (x_{Bj} fixed) limit, the above process is referred to as deep inelastic scattering (DIS). Historically, DIS has been regarded as an extremely useful tool to study the electromagnetic structure of nucleons and nuclei in terms of their underlying quark and gluon degrees of freedom. Understanding nucleon structure and dynamics in terms of quarks and gluons has been a major focus of experimental and theoretical efforts for over twenty years. Even before the emergence of the quark model, elastic electron scattering from nucleons showed that the charge distributions of the proton and neutron extend over a distance of approximately 1 fm. Moreover, pioneering deep inelastic experiments at SLAC in the late 1960's gave the first indication of point-like constituents in the nucleon. Experimentally, deep inelastic lepton-nucleon interactions could be understood if the nucleon was composed of point-like scattering

Table 1.1: Kinematic variables in semi-inclusive leptoproduction.

Inclusive variables

$E_\ell(E'_\ell)$	Energy of incident (scattered) lepton in lab
$Q^2 \equiv -q^\mu q_\mu$	Negative invariant mass squared of exchanged photon
$\nu \equiv \frac{q^\mu P_\mu}{\sqrt{P^\mu P_\mu}} \stackrel{\text{lab}}{=} E_\ell - E'_\ell$	Energy of exchanged photon in lab
$y \equiv \frac{q^\mu P_\mu}{k^\mu P_\mu} \stackrel{\text{lab}}{=} \frac{\nu}{E_\ell}$	Fraction of lepton's energy lost in lab $(0 < y < 1)$
$x_{Bj} \equiv \frac{-q^\mu q_\mu}{2q^\mu P_\mu} = \frac{Q^2}{2M_N\nu}$	Bjorken scaling variable $(0 < x_{Bj} \leq 1)$
$W^2 \equiv (q^\mu + P^\mu)^2 = M_N^2 + \frac{Q^2(1-x_{Bj})}{x_{Bj}}$	invariant mass squared of final hadronic state; total energy squared in $\gamma^* N$ cms

Hadronic Variables

$E_h(E_h^*)$	Energy of hadron in lab ($\gamma^* N$ cm) system
$z \equiv \frac{q^\mu h_\mu}{q^\mu P_\mu} \stackrel{\text{lab}}{=} \frac{E_h}{\nu}$	Fraction of photon's energy carried by hadron in lab $(0 \leq z \leq 1)$
$p_t(p_{\|\|})$	Transverse (longitudinal) momentum of hadron with respect to photon direction in $\gamma^* N$ cms
$m_t \equiv \sqrt{m_h^2 + p_t^2}$	Transverse mass of hadron
$\eta \equiv \frac{1}{2}\ln(\frac{E_h^* + p_{\|\|}}{E_h^* - p_{\|\|}})$	cms rapidity
$x_F \equiv \frac{p_{\|\|}}{\lvert p_{\|\| max}\rvert} \simeq \frac{2p_{\|\|}}{W} \simeq \frac{2m_t}{W}\sinh\eta$	Feynman-x $(-1 \leq x_F \leq 1)$

centers called "partons". At about the same time, it was proposed that the multitude of hadron states and resonances could be theoretically understood if hadrons consisted of more elementary particles called "quarks". These quarks were later identified with partons and today we are very confident that the quark picture of matter is correct.

The early DIS experiments also showed that quarks, which carry charge, comprise only roughly half of the nucleon's momentum. Thus, there is a substantial uncharged component in the nucleon, which was later identified with the gluons predicted by Quantum Chromodynamics (QCD). Due to its many successes, QCD remains to this day the accepted gauge theory of the strong interaction.

1.1 Parton Model

Traditionally, the *inclusive* deep inelastic scattering process, where only the scattered lepton is detected, has been interpreted within the framework of the parton model, which provides an extremely simple picture of the nucleon as probed by the DIS process. In the DIS limit, the asymptotic freedom property of the strong interaction allows us to view the nucleon as a collection of quasi-free, on-shell partons. It should be stressed that our ability to adopt this point of view is independent of the frame chosen. Indeed, both Q^2 and ν are Lorentz invariant. Rather, the motivation for interpreting DIS data in the infinite momentum frame is that momenta transverse to the boost axis, as well as target mass effects, can be ignored. In this case, the Bjorken variable x_{Bj} has a simple interpretation (at leading order): it measures the momentum fraction of the nucleon carried by the struck quark. Moreover, the Lorentz boost slows down processes within the nucleon, making the impulse approximation exact.

1.2 Operator Product Expansion

Of course, the DIS limit where $Q^2 \to \infty$ is only a theorist's dream, since experiments are conducted at finite values of Q^2. Understanding lepton-nucleon scattering at small values of Q^2, say $Q^2 <$few GeV^2, is *a priori* a non-trivial problem. However, very general principles of quantum field theory—more general than QCD itself— give a clear answer for sufficiently large photon virtualities Q^2. The procedure [1, 2, 3], first postulated by Wilson [4], is to solve QCD by factorizing phase space into low and high virtuality regions via the Operator Product Expansion (OPE). The OPE has been demonstrated to apply to all renormalizable theories [1]. One can derive sum rules for the structure functions directly from QCD using the OPE. These sum rules are important because they do not depend on any model of hadronic structure and, consequently, provide a direct test of QCD.

According to the OPE, in coordinate space ξ^μ language, one can write an operator product as an expansion in nonsingular local operators such that any singularities in the operator product $\lim_{\xi^\mu \to 0} \mathcal{O}_a(\xi)\mathcal{O}_b(0)$ can be absorbed completely into the "Wilson coefficients" $c_{abk}(\xi^2)$:

$$\lim_{\xi^\mu \to 0} \mathcal{O}_a(\xi)\mathcal{O}_b(0) = \sum_k c_{abk}(\xi^2)\mathcal{O}_k(0) \tag{1.2}$$

Since QCD is asymptotically free at small distances, the coefficient functions should be free of long-distance contributions and hence perturbatively calculable, as long as all non-perturbative effects occur at scales much larger than ξ, that is $\xi \ll \frac{1}{m}$, where $m \sim \Lambda_{QCD} \sim M_N$ generically represents some hadronic (confinement) energy scale.

Fourier transforming equation 1.2 implies that in four-momentum space ($Q^2 \equiv -q^\mu q_\mu$):

$$\lim_{Q^2 \to \infty} \int d^4\xi^\mu \; e^{iq^\mu \xi_\mu} \; \mathcal{O}_a(\xi)\mathcal{O}_b(0) = \sum_k c_{abk}(Q^2) \; \mathcal{O}_k(0) \tag{1.3}$$

where, again, the coefficients $c_{abk}(Q^2)$ ($Q^2 \gg m^2$) are assumed to be independent of confinement dynamics. The usefulness of this result is clear when we consider that the hadronic structure tensor for, e.g., inclusive scattering, can be written:

$$4\pi W^{\mu\nu} = \int d^4\xi^\mu \; e^{iq^\mu \xi_\mu} \; \langle P, S | J^\mu(\xi) J^\nu(0) | P, S \rangle \tag{1.4}$$

where $|P, S\rangle$ represents the nucleon state with momentum P and spin S. It follows, after some algebra [2, 3], that the OPE gives a direct correspondence between moments of structure functions and nucleon matrix elements of local operators multiplied by perturbatively calculable Wilson coefficients:

$$M^n(f(Q^2)) \equiv \int_0^1 dx_{Bj} \;\; x_{Bj}^n \, f(x_{Bj}, Q^2) \Longleftrightarrow C(Q^2) \cdot \langle P, S|\mathcal{O}(0)|P, S\rangle \qquad (1.5)$$

The above equation clearly illustrates the dual role of DIS, both as a test of QCD and as a probe of (non-perturbative) hadronic structure.

Using dimensional analysis, it turns out that the *twist* (t = mass dimension - spin) of an operator is extremely useful in classifying its dominant contribution to DIS. In particular, the most important operators in the OPE are those with the lowest twist: an operator of twist-t makes a contribution $(\frac{m}{Q})^{t-2}$ to a given structure function moment. Since the fundamental fields in QCD are quark and gluon fields, the operators in the OPE can be written in terms of quark fields, gluon field strength tensors, and an arbitrary number of covariant derivatives. Each quark field or gluon strength tensor contributes one unit of twist. A gauge-invariant operator must be at least twist-2, which corresponds to one quark (or gluon) line in the initial and final states. This is exactly the naive parton model picture of DIS, and indeed only the twist-2 contribution survives in the $Q^2 \to \infty$ limit. Physically, higher twist contributions arise from multi-parton correlation effects involving additional partons (e.g., final state interactions). It is important to distinguish higher twist contributions from higher order contributions, which physically correspond to hard gluon radiation. Unlike higher twist effects, which fall off as an inverse power of Q, higher order effects depend only logarithmically on Q^2.

The OPE description of DIS requires that we interpret the measured structure functions as representing nucleon degrees of freedom. However, it should be realized that these are QCD degrees of freedom that usually have no simple correspondence to the degrees of freedom that we may normally associate with the nucleon [5, 6, 7], such as "constituent" quarks. In particular, only at rather large values of $x_{Bj} \geq 0.1 - 0.2$

does DIS correspond to forward Compton scattering that occurs inside the nucleon volume (in the nucleon's rest frame) [8, 9]. The small x_{Bj} behavior of structure functions corresponds to matrix elements of operators with increasingly large dimensions, and it is conceivable that we will never be able to perform calculations in this region directly from QCD [10, 11]. Hence, in the low x_{Bj} regime, a different dynamical description may be more economical. Indeed, it is already known that in this domain, the Compton scattering amplitude in the nucleon's rest frame is dominated by the photon splitting into a quark-antiquark pair that subsequently scatters off the background color field of the target nucleon [8, 9].

1.3 Spin-Dependent DIS

One of the convincing features of the quark model was that it was able to explain, at the 20% level or better, the magnetic moments of nucleons and hyperons as vector sums of the magnetic moments of constituent quarks, assuming that the latter are Dirac spin-$\frac{1}{2}$ particles. The spin-$\frac{1}{2}$ nature of quarks had already been derived from angular jet distributions in e^+e^- collisions as well as from the approximate validity of the Callan-Gross relation for inclusive structure functions in unpolarized DIS [12]. The success of this approach led to the belief that the spin of the nucleon arises primarily from the spins of its quarks, with negligible contributions from quark orbital angular momenta or gluonic degrees of freedom.

Since the 70's, there has been an experimental program intended to study the spin structure of the nucleon via polarized deep inelastic scattering. The focus until rather recently has been solely on the twist-2 structure function g_1, which is roughly proportional to the inclusive spin asymmetry on a longitudinally polarized target. Due to the apparent success of the parton model in unpolarized scattering, the experimental data have taken the scientific community by surprise. When interpreted within the parton model, data on the first moment of g_1, together with the assumption of SU(3) flavor symmetry, imply that quark spins account for only a fraction, $\Sigma \approx 0.3$, of the nucleon spin. This has been often termed the "spin crisis".

However, within QCD there is no reason whatsoever to expect that Σ should be close to unity [6]. Firstly, this expectation is based upon a static, constituent quark model of the nucleon, whereas it is known that there is no clear correspondence between constituent quark degrees of freedom and those probed by the DIS process. Moreover, it is now widely acknowledged [13, 14] that contributions from quark orbital angular momenta and gluon polarization are likely to be significant. Even in very simple models of the nucleon, such as the bag model, relativistic effects reduce the quark helicity contribution to Σ by roughly a factor of $\frac{2}{3}$ [6].

Furthermore, it is unclear whether Σ should even be interpreted as the quark helicity contribution to the spin of the nucleon. More precisely, $\Sigma(\mu^2) = \sum_{f=u,d,s} \Delta q_f(\mu^2)$ is the SU(3) singlet combination of spin-dependent parton distributions in a longitudinally polarized nucleon, where within the framework of OPE, the $\Delta q_f(\mu^2)$ are related to matrix elements of the quark axial-vector current

$$\Delta q_f(\mu^2) \propto \langle P, S | j^{\mu}_{5\,f} | P, S \rangle \tag{1.6}$$

In fact, there are good arguments [15, 16] in favor of the view that the quark axial charges defined above are contaminated *at leading order* by $\Delta g(\mu^2)$, the contribution of polarized gluons to the nucleon spin. A possible gluonic contribution to the nucleon's axial charge and a method to extract it experimentally are discussed in Chapter 4. More generally speaking, the quark axial charges are *not* renormalization scale invariant. Hence, it has been argued [16] that it is misleading to regard $\Sigma(\mu^2)$ as the spin fraction of quarks; it is not a fixed number and can, in principle, have any value whatsoever, depending on the renormalization scale μ^2. Consequently, only in the parton model, with additional assumptions about the negligible role of gluons and quark orbital momenta, is there a spin problem [6, 16]. An experimental determination of the relative contributions from these additional degrees of freedom is a major focus of the latest generation of existing and proposed spin physics experiments.

1.4 Motivations for Semi-Inclusive DIS

Semi-inclusive scattering offers several unique advantages over the inclusive reaction alone. Firstly, the detection of various hadrons in coincidence with the scattered lepton allows to probe directly the *flavor* dependence of structure functions, and consequently, of certain QCD operators of interest. For example, a global analysis of the existing data on g_1 implies that strange quarks may be substantially polarized in the nucleon. Hence, much interest has been focused on the possibility to measure the role of strange quarks in the polarized structure of the nucleon. Strange quark observables are also particularly interesting because they are sensitive to more exotic aspects of the nucleon's wavefunction.

Moreover, semi-inclusive measurements allow to probe the *charge* structure of distribution functions. Since DIS is a charge conjugation even ($C+$) process, inclusive measurements allow extraction of matrix elements of $C+$ operators only. That is, they do not distinguish between quark and antiquark degrees of freedom. On the other hand, in semi-inclusive reactions $C-$ distribution functions can, for example, couple to $C-$ fragmentation functions. In the most general case, as discussed in Chapter 3, the distribution functions extracted from semi-inclusive reactions have mixed charge symmetry.

It is often claimed that $C-$ (quark) distribution functions measure the degrees of freedom of valence quarks. Strictly speaking, this is incorrect. This follows from the fact that there is no way to physically separate valence and sea degrees of freedom, except for *defining* the sea to be charge conjugation even [17]. On the other hand, this assumption is completely unfounded in QCD, as there is no symmetry in the Lagrangian that allows one to relate quark and antiquark degrees of freedom in the nucleon [17, 18]. Note that, indeed, the *hard* gluon splitting process $g \to q\bar{q}$ that generates sea quarks is charge symmetric ($C+$). On the other hand, the subsequent evolution of the quark and antiquark states is governed by confinement scale physics that reflects that nucleon state, which has $C-$ symmetry. At the level of Feynman diagrams, for each quark interaction there is a corresponding diagram involving an antiquark, with the same probability. On the other hand, the phase factors are not necessarily equal. When considering the long time scale evolution that reflects non-perturbative nucleon dynamics, the various amplitudes will generally interfere to produce quark distribution functions that lack any definite charge symmetry properties.

Semi-inclusive measurements are also interesting because they allow the measurement of polarization observables in the hadronic final state, particularly pseudovector observables, such as Λ (vector) polarization [19, 20, 21], hadron azimuthal asymmetries [22, 23], and jet handedness [24], that can in principle couple to the polarization of current quarks (and gluons) in the nucleon. Finally, semi-inclusive DIS processes are more complete experimental measurements than the inclusive scattering reaction. Hence, it may be anticipated that they will provide more stringent insights into the relevant reaction mechanisms, and more generally, into the most economical way in which to view the photon-nucleon system at high energies.

The extraction of polarized quark distribution functions from spin-dependent semi-inclusive reactions requires an understanding of parton-hadron correlations that characterize the hadronization process. Chapter 3 presents a coherent treatment of the connection between partonic and hadronic degrees of freedom, relevant to the HERMES experiment (described in Chapter 2). As an application of the ideas presented there, a formalism is introduced that allows one to relate quark spin distributions to the semi-inclusive asymmetries accessible at HERMES, or more generally, at any experiment with sufficient hadron identification.

Chapter 2

The HERMES Experiment

HERMES is a new experiment at the HERA accelerator at DESY (Deutsches Elektronen-Synchrotron, Hamburg, Germany). Commissioned in 1995, its primary purpose is to study, in a more complete way than its predecessors at SLAC and CERN, the spin structure of the nucleon by deep inelastic scattering of 27.5 GeV polarized positrons off polarized nuclear targets. HERMES makes use of two novel techniques: a longitudinally polarized positron beam in a storage ring and a pure internal polarized gas target. This allows for a rather clean experimental environment, with little dilution by unpolarized gas nuclei. Furthermore, as a second generation spin structure experiment, HERMES has been designed to identify various hadronic final states, allowing the study of semi-inclusive processes.

2.1 The HERA Accelerator Facility

The HERA facility, which contains storage rings for 820 GeV protons and 27.6 GeV positrons (or electrons), was primarily constructed for the collider experiments, ZEUS and H1, which are situated in the South and North Halls, respectively. From the point of view of HERMES, located in the East Hall, the choice of the storage ring was mainly determined by the requirements of fast polarization build-up (approximately 30 min) and high beam currents (up to 35 mA). The East Hall was originally foreseen to contain a possible third collider experiment. For HERMES, the lepton and proton beams have been separated by 72 cm and run in different beam pipes, ensuring that the proton beam conditions are not affected by the operation of the HERMES internal target. All three experiments are able to take data simultaneously during the full time of beam operation. Currently, HERA runs positrons due to the longer beam lifetime; an electron beam has been found to have a significantly reduced lifetime due to ionized dust particles that are captured due to their positive charge.

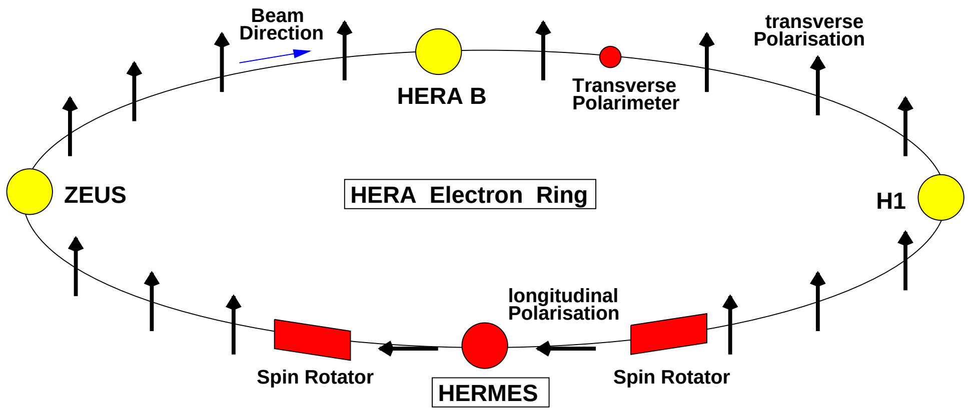

Figure 2-1: The HERA ring with the HERMES spin rotators.

HERA is the world's first high energy lepton storage ring to achieve longitudinal polarization [25, 26]. The polarization of the leptons is naturally caused by the Sokolov-Ternov effect [27]: the synchrotron radiation process contains a small asymmetric spin-flip amplitude that enhances the polarization state anti-parallel to the magnetic fields of the bending magnets. Since HERMES requires longitudinal beam polarization, spin rotators located before and after the interaction point are used to rotate the spin of the beam (see Figure 2-1).

The beam polarization is measured using laser backscattering Compton polarimeters [28]. Initially, the polarization was measured only with a transverse polarimeter located in the West Hall, with the assumption that the polarization is longitudinal, to within a few degrees, at the HERMES interaction region. Recently, a longitudinal polarimeter has been constructed at the East Hall to check this assumption and to reduce the systematic error of the polarization measurement. Figure 2-2 shows the first observation of longitudinal polarization at HERA. Since then, polarization values

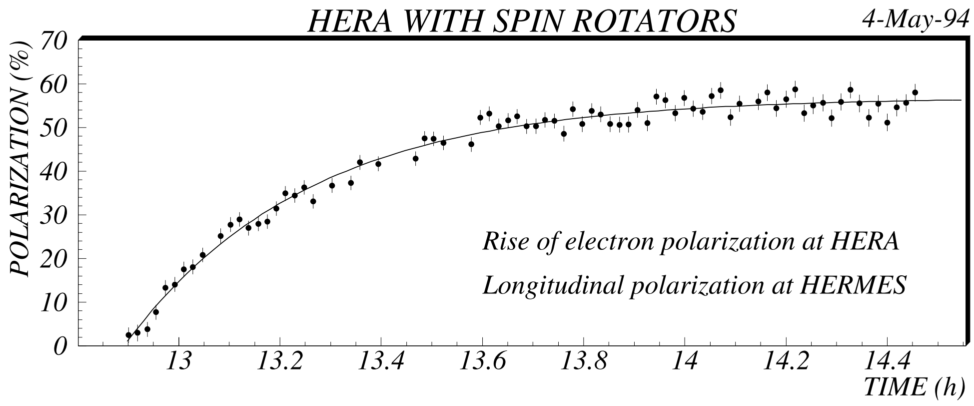

Figure 2-2: The first observation of longitudinal polarization at HERA.

of up to 70% have been achieved.

2.2 HERMES Polarized Targets

From the experience of previous spin structure experiments, it was clear that a major source of systematic errors originated from the large dilution factors, and consequently long spin-reversal times, of external targets. Therefore, HERMES has decided to utilize internal gas targets as they can be polarized to a high degree without significant dilution by unpolarized nuclei; they also allow for rapid polarization reversal, which is instrumental in reducing time-dependent systematic errors in spin asymmetry measurements. High luminosity is achieved by using the novel technique of a storage cell, in which polarized gas is fed into a T-shaped elliptical cell. Since gas atoms typically undergo several hundred wall bounces before leaving the cell, the density of the gas is increased by roughly two orders of magnitude compared to a free gas jet. The low gas pressure means that very thin cell walls can be used, which greatly minimizes corrections due to external radiative corrections and multiple scattering. By additionally cooling the storage cell to low temperatures, the target density can be further increased. At HERMES, the target thickness is typically of order $10^{14} - 10^{15}$ polarized atoms/cm^2. A diagram of the HERMES storage cell is shown in Figure 2-3.

Two different types of polarized gas sources have been used at HERMES thus far:

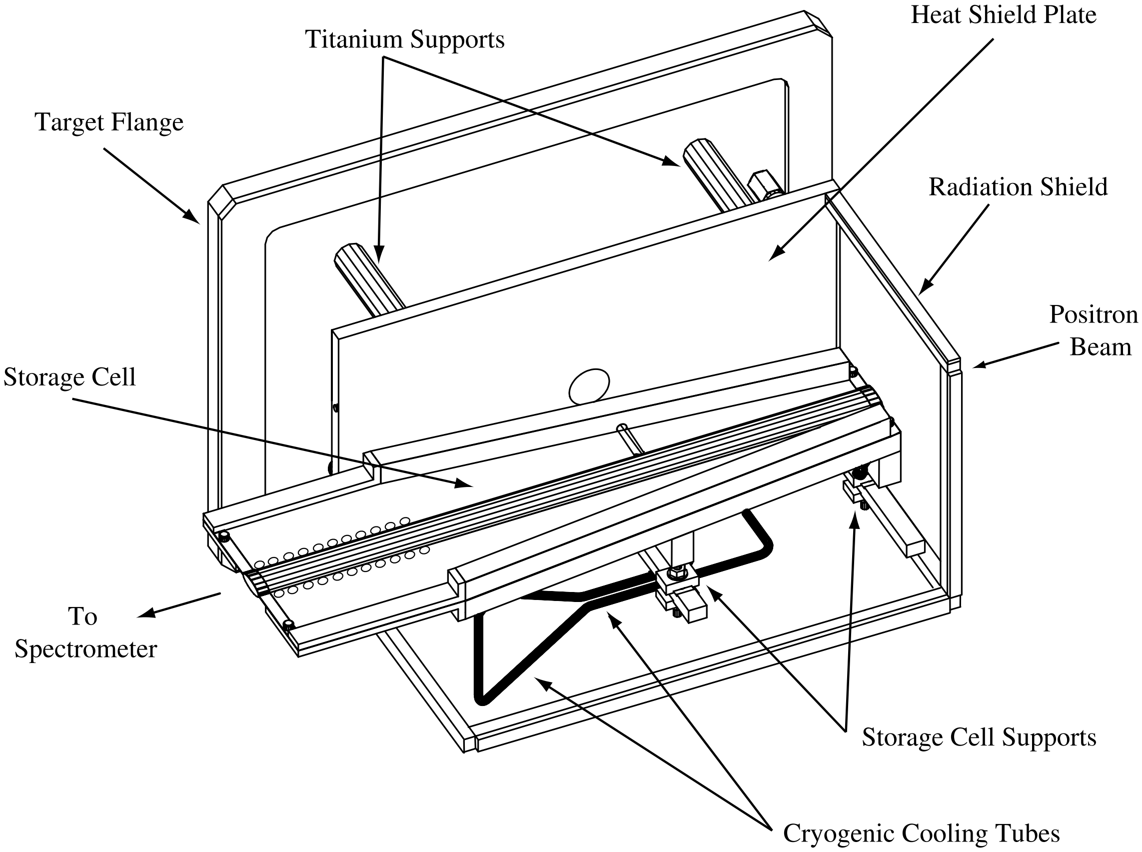

Figure 2-3: The HERMES cryogenic target cell.

an optically pumped source for ^3He [29] and atomic beam source [30] for hydrogen and deuterium. Additionally, a laser driven source [31] for hydrogen and deuterium is currently under development that could have a much increased intensity compared to the existing atomic beam source.

In 1995, data were taken using a polarized ^3He target, which achieved polarizations of roughly 50-60%. Polarized targets of ^3He have become widely used in the last several years for spin-dependent measurements on the neutron. Since the ^3He nucleus is mostly in a spatially symmetric S-state, antisymmetrization of the nuclear wavefunction requires that the two proton spins are anti-aligned; hence, a polarized ^3He nucleus is essentially a polarized neutron. Nuclear polarization is achieved via a metastability-exchange pumping technique. Atoms of ^3He are excited from the 1^1S_0 electronic ground state into the metastable 2^3S_1 state via an radio frequency dis-charge. Atoms in the metastable state can be optically pumped through the 1083 nm transition to the $2^3P_{0,1,2}$ levels. By using circularly polarized light, orbital angular momentum is transferred to the system, and the ^3He atomic system becomes polarized. Subsequent metastability-exchange collisions with ground state ^3He atoms produce populations of polarized ground state atoms. Polarization transfer to the nuclei occurs via the hyperfine interaction.

Currently, HERMES uses a target based on an atomic beam source that produces hydrogen beams with polarizations of better than 90%. A Stern-Gerlach separation of magnetic substates is achieved by passing the atomic beam through a sextupole magnetic field. Consequently, radio frequency transitions are induced between hyperfine states of the atoms to select different nuclear polarization states and to provide rapid spin reversal.

2.3 The HERMES Detector

The HERMES detector is a large-acceptance, forward spectrometer (see Figure 2-4) primarily designed to provide clean identification of the scattered positron in a wide kinematic range and with good angular and momentum resolution. Additionally, it has been designed to provide good particle identification of hadronic final states in the forward direction. The range of accepted scattering angles is roughly $40\ mrad < \theta < 200\ mrad$.

A top view of the spectrometer, indicating the positions of the various detector subcomponents, is shown in Figure 2-5. A large-gap, H-type magnet is used to provide a dipole field with integrated strength of 1.3 T-m. Both the positron and proton beam pipes pass through an iron septum plate that shields them from the influence of the field. In combination with the magnetic field, tracking chambers before (Silicon Vertex Chambers VC1-2 and Front Drift Chambers FC1-2) and after (Back Drift Chambers BC1-4) the magnet are used to determine particle momenta and signs of charge. Additionally, low-resolution proportional chambers inside the

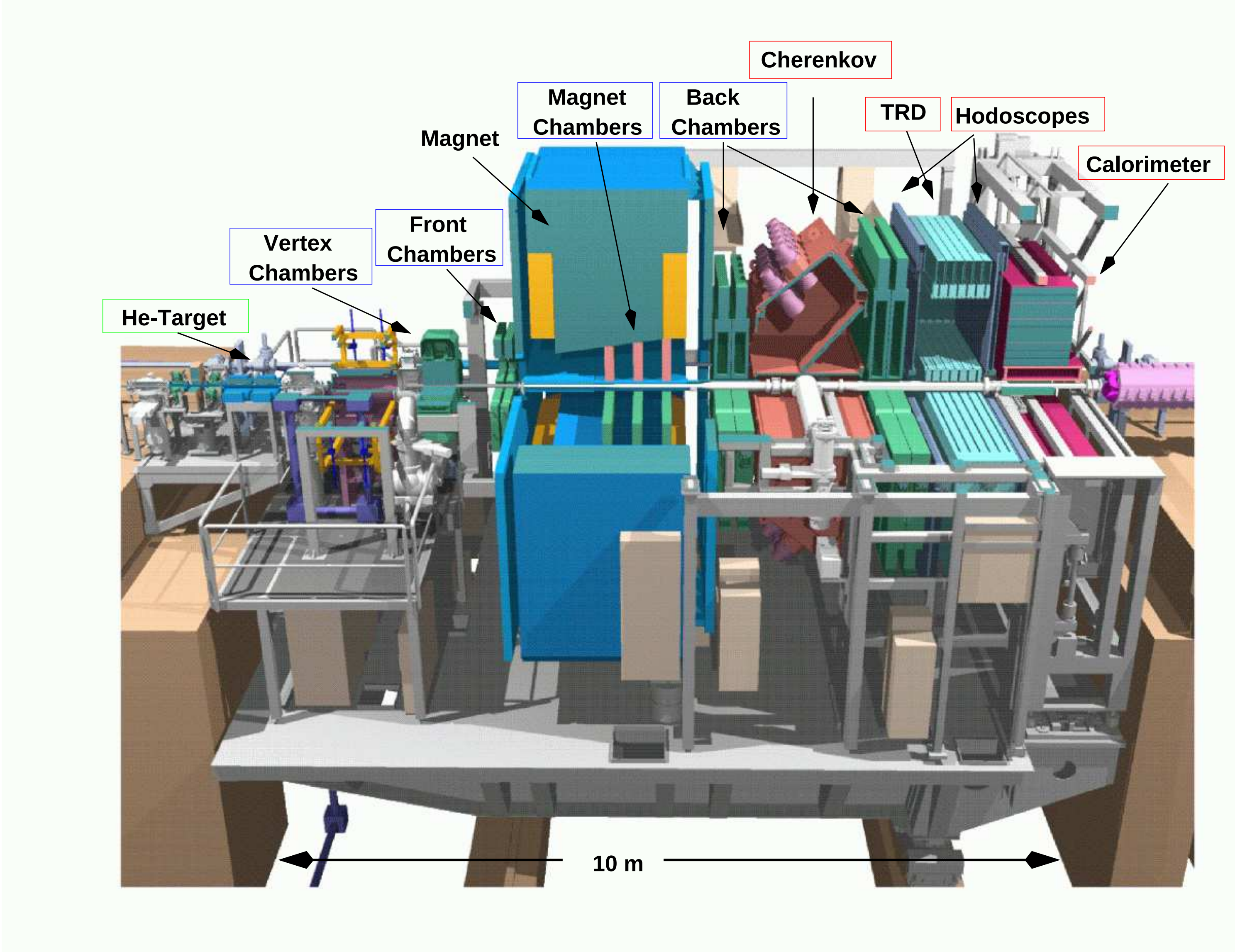

Figure 2-4: Three-dimensional representation of the HERMES detector.

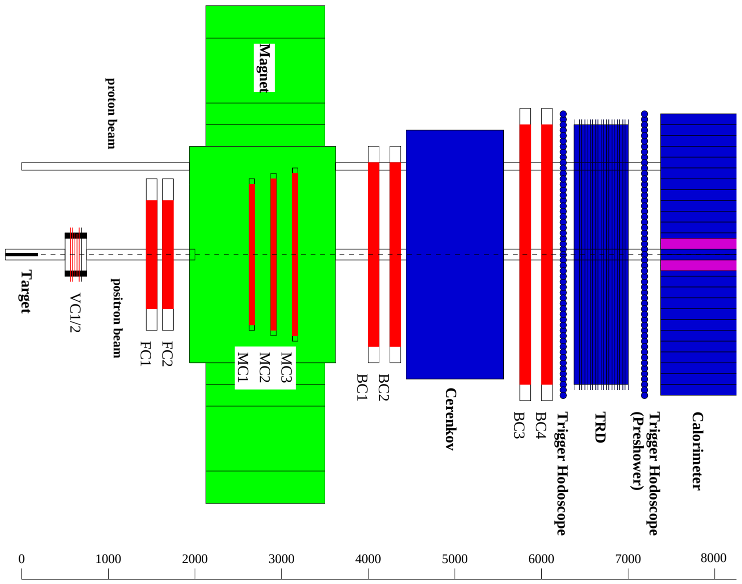

Figure 2-5: Schematic view of the detector components in the HERMES spectrometer.

magnet (Magnet Chambers MC1-3) were added to aid in case of problems in track reconstruction for high multiplicity events.

A clean separation of positrons from hadrons, especially pions due to photoproduction processes, is accomplished by using the combination of a segmented electromagnetic calorimeter (CAL), a preshower detector (H2), and a transition radiation detector (TRD). Since the nuclear reaction length of the calorimeter is much larger than the electromagnetic radiation length, charged hadrons (mostly pions) cause larger clusters in the calorimeter than the scattered positrons. Hence, a comparison of energy deposited in the calorimeter with the momentum determined via tracking provides a way to separate charged hadrons and positrons. Directly upstream of the calorimeter is a preshower that consists of a 1.1 cm thick lead sheet followed by a vertical array of plastic scintillator paddles; each paddle covers one vertical column of lead glass blocks in the calorimeter. The preshower-calorimeter combination improves the hadron rejection factor of the calorimeter alone by roughly a factor of 50. The transition radiation detector, which utilizes the radiation generated at the boundary between media of different refractive indices, essentially measures the relativistic γ factor for charged particles. By itself, it provides a very good hadron rejection factor of well over 10^3.

The first-level trigger for inclusive or semi-inclusive events consists of a coincidence between the calorimeter (CAL), the preshower counter (H2), and the first hodoscope (H1). The H1 hodoscope, due to its short radiation length, provides a photon rejection factor of 50 to 1. This is useful to remove triggers by high energy photons, e.g., from π^0 decay. Additionally, the combination of H1 and H2 hodoscopes can be used for time-of-flight particle identification for energies up to roughly 2 GeV. A threshold Čerenkov counter, located between the two sets of back chambers, provides partial proton-kaon-pion separation. A dual-radiator Ring-Imaging Čerenkov (RICH), to be installed during the 1997-1998 Winter shutdown, is currently being built to allow full proton-kaon-pion separation over essentially the entire kinematic range. Even in the first year of running, however, the somewhat redundant tracking and particle identification capabilities at HERMES have allowed for the reconstruction of various decaying particles (e.g., π^0, ω, η, ϕ, ρ^0, Λ, K_s^0, K^*, J/ψ). It is expected that a global analysis of the hadronic final states accessible at HERMES will provide key information on the charge and flavor structure of parton distributions. A general formalism that allows one to relate quark spin distributions to an arbitrary combination of semi-inclusive asymmetries is introduced in the next Chapter.

Chapter 3

Quark Flavor Tagging

3.1 Introduction

In the $\gamma^* N$ center-of-mass system (cms), the struck quark and target remnant each have an energy of $W/2$ and will move roughly back-to-back with rapidities $\eta \sim \pm \ln W$, respectively. Due to the confinement property of QCD, we do not observe partons (quarks and gluons) in the final state. Rather, the struck quark and target remnant system will fragment into hadrons with rather small $\langle p_t \rangle \sim 0.35\ GeV$. At sufficiently large values of W, hadrons associated with the struck quark (current fragmentation) will be kinematically confined to the forward region ($\eta, x_F > 0$), while hadrons associated with the target remnant (target fragmentation) will be found predominantly in the backward region ($\eta, x_F < 0$). The intervening region around $\eta = 0$ is called the central region, or hadronic plateau (see Figure 3-1). The essential feature of the central region is that it is independent of both the struck quark and target remnant, or more generally, projectile and target. Hence, we expect that hadronic spectra in the central region will be universal for all hadronic reactions, independent of the nature of incoming particles, at fixed center of mass energy W. This expectation has been confirmed experimentally in hadron-hadron collisions [32]. Moreover, and perhaps even more surprising, hadron energy spectra in the central region are found be very similar in pp, $p\bar{p}$, photoproduction, and low-x_{Bj} DIS processes [33]. These global features of final state hadrons in high-energy processes can be easily understood in terms of the hypothesis of *short range correlations* in rapidity [34].

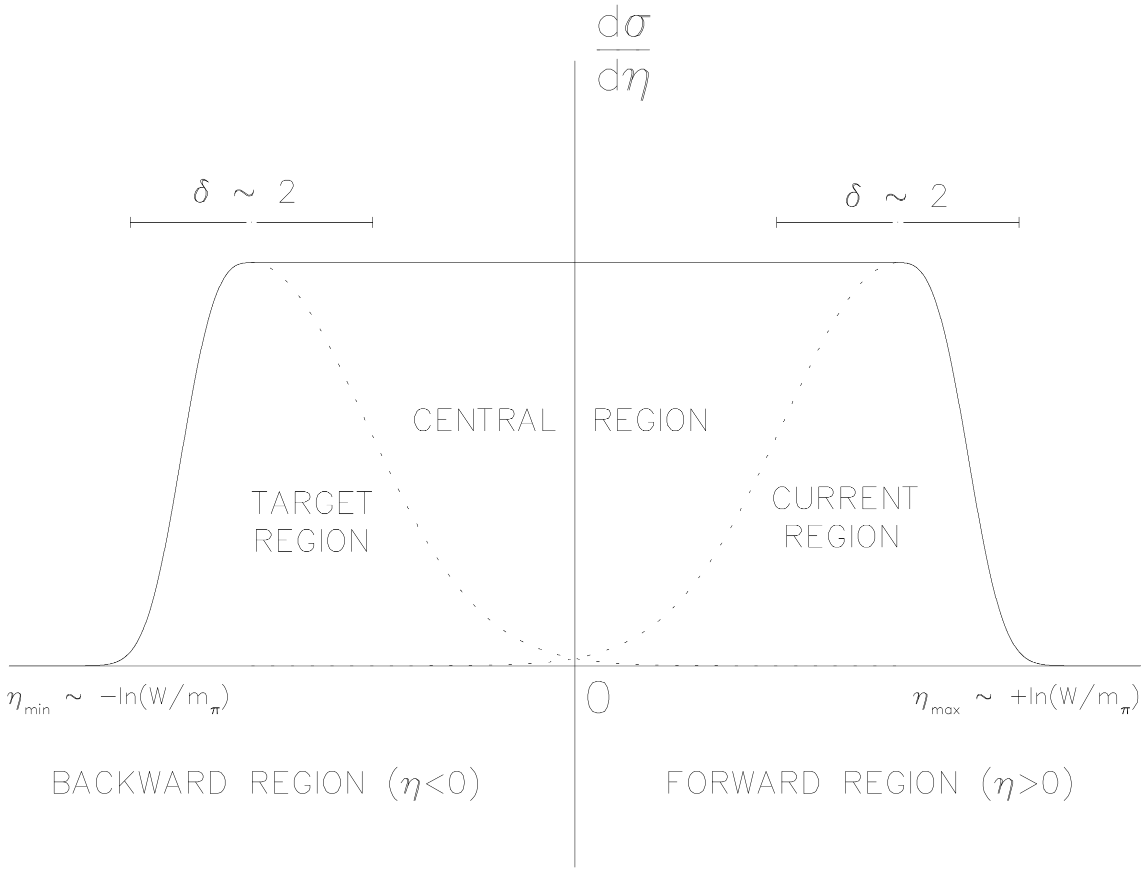

Figure 3-1: Illustration of typical hadronic rapidity distribution.

The fragmentation process, where colored partons are transformed into colorless hadrons, is governed by long distance ($r \sim \frac{1}{\Lambda_{QCD}}$) dynamics, where perturbation theory breaks down. It has yet to be understood from first principles, starting with the *QCD* Lagrangian. Instead, it is necessary to resort to phenomenological models that attempt to capture the gross physical features. A review of the status of fragmentation models may be found in [35, 36]. The general approach to fragmentation is the hypothesis of *local parton-hadron duality* (LPHD) [37, 38], where it is assumed that the flow of momentum and quantum numbers at the hadron level tends to follow the flow established at the parton level. Quantitative agreement between calculated parton spectra and measured hadron distributions has been confirmed in e^+e^- [38, 39]

and DIS [40] processes. Hence, in the current fragmentation region, one expects a large correlation between the flavor of the struck quark and the types of produced hadrons, in particular, hadrons whose valence quarks contain the flavor of the struck quark. The existence of such a correlation is necessary in order for quark flavor tagging to work. It is therefore worthwhile to study the interplay between the different fragmentation regions, and in particular the kinematical dependence of parton-hadron correlations.

3.2 Parton-Hadron Correlations

A clean separation between the current and target fragmentation regions is typically regarded as a necessary criterion for quark flavor tagging. Quantum mechanically, the question of whether or not an observed hadron contains the struck quark is not well defined. However, it is appropriate, and from a phenomenological point of view sufficient, to discuss correlations (e.g., flavor correlations) between the observed hadrons and the underlying partons. The primary goal of this section is to quantify the kinematical dependence of hadron correlations with the struck quark and with the target remnant. In Section 3.3 of this Chapter, consequences of target "contamination" for flavor tagging are discussed in the context of a nucleon spin decomposition from hadron asymmetries.

3.2.1 Berger Criterion

The issue of current/target separation has already been addressed by Berger [41]. The argument is briefly summarized here. The full range of rapidity η allowed kinematically is roughly $\Delta\eta \equiv \eta_{max} - \eta_{min} \sim \ln W^2$ (see Table 1.1). Also, the typical hadronic correlation length in rapidity is taken to be $\delta \simeq 2$. Hence, for separate current and target regions, it is necessary that $\Delta\eta \geq 2\delta$, or, equivalently, that $W \geq 7.4\ GeV$. In this case, the forward region ($0 < x_F < 1$) should contain only current fragmentation. However, this derivation neglects transverse mass effects, which are especially important at HERMES kinematics ($W < 7\ GeV$). In addition, parton-hadron correlations need to be treated in a more complete way in order to obtain a quantitative estimate of target contamination, which is done below.

It has also been argued in [41] that smaller values of W may be used if the minimum x_F (or z) is increased. Several examples of (x_F,W) cuts are given on the basis of scaling violations in inclusive charged-particle momentum spectra measured in e^+e^- collisions [42]. However, as discussed in [42, 12], these scaling violations are due to threshold production of charmed particles, where, as expected, the region of scaling extends down to lower values for x_F as the center of mass energy W (mass threshold) is increased. It is doubtful, therefore, whether there is any relation to separation of current and target fragmentation regions.

3.2.2 More Realistic Treatment

Consider a hadron at fixed kinematics (x_F,W,p_t). It is clear that its rapidity differences relative to the struck quark $\Delta\eta^q$ and relative to the target remnant $\Delta\eta^r$ are given by (see Table 1.1):

$$\Delta\eta^q \simeq \sinh^{-1}(\frac{Wx_F}{2m_t}) - \sinh^{-1}(\frac{Wx_F^q}{2m_t^q}) \tag{3.1}$$

$$\Delta\eta^r \simeq \sinh^{-1}(\frac{Wx_F}{2m_t}) - \sinh^{-1}(\frac{Wx_F^r}{2m_t^r}) \tag{3.2}$$

Neglecting hard gluon bremsstrahlung and hadronization effects, x_F^q and x_F^r are roughly equal to ± 1, respectively. The goal of this section is to answer two questions: 1) What is the correlation of the detected hadron with the struck quark? 2) What is the correlation of the detected hadron with the target remnant?

To obtain quantitative answers to these questions, it is convenient to introduce, in the spirit of LPHD, a parton-hadron correlation function $\Phi(\Delta\eta, \delta)$, which is assumed to be Gaussian and depend only on rapidity differences [43], as calculated above:

$$\Phi(\Delta\eta, \delta) = \exp\left[-(\frac{\Delta\eta}{\delta})^2\right] \tag{3.3}$$

In the above equation, δ is the correlation length, which may depend on particle masses [43]. Hadronic rapidity correlations in fragmentation are well established. Two-hadron rapidity correlations have been measured in e^+e^- [44], hadronic [45], and DIS [46, 47] experiments. The correlation functions are found be be roughly Gaussian, with $\delta \simeq 1-2$. In particular, the rapidity distribution of the hadronic net charge in DIS [47], with the cut $10 < W < 20\ GeV$, shows the following features: 1) Target and current regions are well separated, with almost no net charge in the central region, as expected; and 2) The widths of the current and target fragmentation peaks are roughly 2 units of rapidity. In addition, the shape of the hadronic net charge distribution is expected to be well approximated by the product of the parton-hadron correlation function (eqn. 3.3) and the hadronic rapidity spectrum. Using the rapidity spectra published in [48], which were obtained with the same apparatus and at the same kinematics as the data in [47], implies that the choice $\delta \simeq 2$ is appropriate. This result will be used throughout the subsequent calculations.

Define the *current correlation* $C(x_F, W)$ and *target correlation* $T(x_F, W)$ by the following formulae:

$$C(x_F, W) \equiv \int dp_t dp_t^q N(p_t) \tilde{N}(p_t^q) \Phi(\Delta\eta_q) \tag{3.4}$$

$$T(x_F, W) \equiv \int dp_t dp_t^r N(p_t) \tilde{N}(p_t^r) \Phi(\Delta\eta_r) \tag{3.5}$$

where N and $\tilde{N}$ are normalized transverse momentum distributions, obtained from the *PEPSI* [49] Monte Carlo. Note that, due to the existence of the central region, it is not necessary that $C + T = 1$.

The quantities $C(x_F, W)$ and $T(x_F, W)$ have been numerically calculated for pions, which comprise the bulk of HERMES semi-inclusive data. The results are shown in Figure 3-2. Note that, due to the small pion mass, $z \simeq x_F$ for $x_F > 0.1 - 0.2$. As expected, the target contamination decreases as either x_F or W is increased. The decrease of the current correlation as $x_F \to 0$ is of course related to the fact that the ratio of favored to unfavored fragmentation functions becomes roughly unity at small

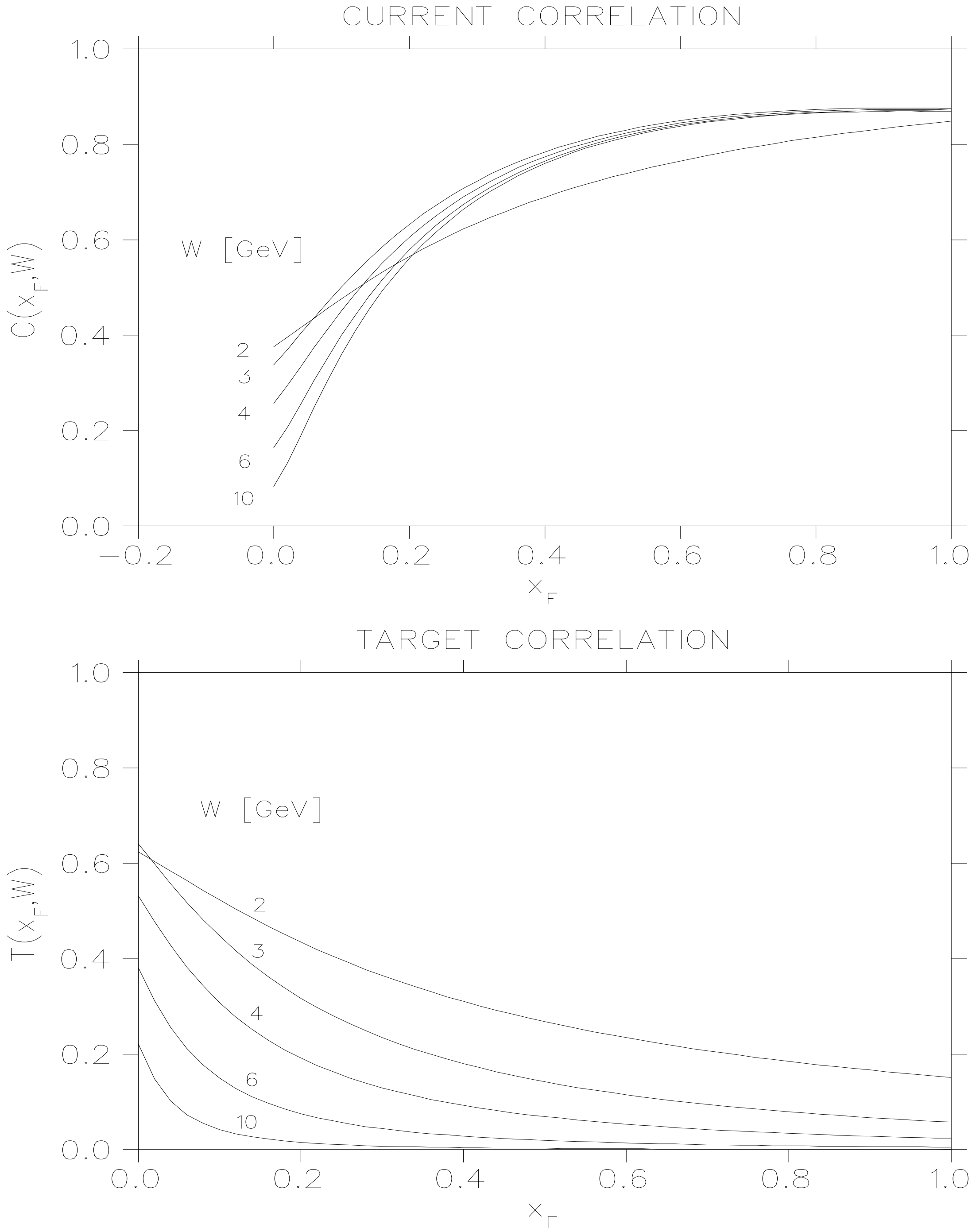

Figure 3-2: Correlations, as a function of x_F and W, of the observed pions with respect to the struck quark $C(x_F, W)$ and the target remnant $T(x_F, W)$.

x_F. This is expected, since the fragmentation function D_f^h becomes essentially independent of f in the central region. It is useful to note that at small $|x_F| < 0.1$, both the current and target correlations decrease as W *increases*. This implies that most of the increase in pion production with increasing W occurs in the central region. The same results are also found experimentally in DIS [48]: the charged pion fragmentation function $D^\pi(x_F, W)$ rises with W (over the measured range $4 < W < 20$ GeV) at small $|x_F| < 0.1$, but remains constant at higher $|x_F|$, both in the forward and backward regions. Since the height of the central region is roughly independent of W and its width (in rapidity) increases as $\ln(W^2)$, it is natural to expect that the mean charged multiplicity should increase linearly with $\ln(W^2)$, which is indeed observed experimentally [40, 48].

It should be stressed that the W dependence of $C(x_F, W)$ and $T(x_F, W)$ is due to the fact that the central region has been taken into account. If the central region had been ignored (i.e., $C + T = 1$), then the results would have been nearly independent of W. As an example of this, consider hadrons at small $|x_F|$. When W is very small, the current and target fragmentation regions overlap substantially, yielding $C \sim T \sim \frac{1}{2}$. At very large W, on the other hand, the hadrons are uncorrelated with both the struck quark and target remnant, so that C,$T \to 0$, as is seen in Figure 3-2. However, requiring that $C + T = 1$ (i.e., dividing the central region equally between current and target regions), yields $C \sim T \sim \frac{1}{2}$, independently of W. Since the central region is an important aspect of fragmentation, even at HERMES kinematics (small $W \leq 7$ GeV), it needs to be considered when discussing the issue of current/target separation.

The magnitude of target contamination has been also studied with the *PEPSI* Monte Carlo, using the independent (Field-Feynman) fragmentation model, where a clear distinction between target and current fragmentation events is possible. Since, in this case, each hadron is associated with either the struck quark or the target remnant, it is clear that $C + T = 1$. Then, as expected from the above considerations, it is found that the correlations extracted in this way are nearly independent of the center-of-mass energy W. The following results are obtained from Monte Carlo and our calculation above, for fixed x_F and W:

- Target contamination is independent of hadron energy and angle in the lab. Hence, it is unaffected by detector acceptance.
- It is nearly independent of leptonic variables Q^2 and x_{Bj}.
- Current correlation decreases with increasing p_t. In the calculation above, the target correlation also decreases, but to a lesser extent due to the typically larger mass of the target remnant.

3.3 Consequences of Target Contamination

Theoretically, the different fragmentation regions are distinguished by the 'hardness' (e.g., $|x_F|$ or z) of the detected hadron (outgoing parton) and its collinearity with the target remnant [50]. This collinearity leads to a divergence in the cross section that cannot be absorbed into the parton distribution or fragmentation functions. Therefore, to describe target fragmentation, it is necessary to introduce new functions, called *fracture functions* M_f^h [51], which have explicit x_{Bj} dependence and satisfy the momentum sum rule:

$$\sum_h \int dz\, z M_f^h = (1 - x_{Bj}) \cdot q_f \tag{3.6}$$

Hence, it is quite likely that fracture functions significantly violate charge-isospin conjugation symmetry, which is usually assumed to be valid for the current fragmentation functions D_f^h.

It is acknowledged in the theoretical literature [51] that there also exists a kinematical region, i.e., the central region, in which the observed hadrons cannot be unambiguously associated with either the struck quark or the target remnant. However, since the central region is intrinsically "soft" (small $|x_F|$), it is generally ignored in discussions of fragmentation. On the other hand, it has been shown in the previous section that the central region is an important—and often dominant—aspect of fragmentation. Moreover, the correct kinematical behavior of current and target correlations (in particular, their W dependences) will be reproduced only if the central region is taken into account. Hence, many of the existing analyses of target contamination, which ignore the phenomenological consequences of the central region, are incomplete.

Consider a single-hadron, semi-inclusive spin asymmetry, which at leading order in *direct* DIS can be written:

$$A^h = \frac{\sum_f e_f^2 \, \Delta q_f \; D_f^h}{\sum_f e_f^2 \; q_f \; D_f^h} \tag{3.7}$$

In writing eqn. 3.7, it has been also assumed that the fragmentation functions are independent of the helicity of the struck quark. This assumption is justified for any single-hadron, $\vec{p}_t$- and hadron polarization-integrated fragmentation function, since in this case there is no pseudovector observable in the final state that can in principle couple to the polarization of the struck quark. It is typically believed that in the current region, fragmentation functions will not depend on x_{Bj}. However, as discussed in the previous section, even in the absence of target contamination, fragmentation functions exhibit W dependence at small $x_F < 0.1 - 0.2$. Since x_{Bj} and Q^2 are highly correlated in any experiment, and both are related to W via the equation:

$$W^2 = M_N^2 + \frac{Q^2(1 - x_{Bj})}{x_{Bj}} \tag{3.8}$$

it is possible that there will be a residual x_{Bj} dependence in the fragmentation functions, at small $x_F < 0.1 - 0.2$. In general, fragmentation functions also have explicit Q^2 dependence due to QCD radiative corrections. Significant Q^2 variations (at fixed W) have been observed in DIS [52] at small values of $z < 0.2 - 0.3$.

Consider the asymmetry in a kinematic region where target fragmentation is significant. In this case, the asymmetry is still given by eqn. 3.7, provided we make the substitution

$$D_f^h \longrightarrow D_f^h + T_f^h \equiv \tilde{D}_f^h \tag{3.9}$$

where T_f^h are the effective target fragmentation functions. However, from a phenomenological point of view, the only relevant fragmentation functions are the ones that couple to the quark distributions, that is, $\tilde{D}_f^h$. Hence, *there is no reason to exclude the target region, as long as one uses the correct fragmentation functions* $\tilde{D}_f^h$. By construction, the $\tilde{D}_f^h$ contain all phenomenologically relevant information about the fragmentation process (i.e., flavor correlations between struck quark and observed hadrons). Once they are known, they can be used for flavor tagging, our ignorance of the underlying fragmentation dynamics notwithstanding. One can measure them experimentally (using *unpolarized DIS*), preferably in the same kinematical region in which the asymmetries will be measured, or one can calculate them using an assumed fragmentation model.

It is important to realize that, since the same fragmentation functions couple to both $q_f^\uparrow$ and $q_f^\downarrow$, the presence of target fragmentation does not dilute the asymmetry. Even in the target region, one expects to observe an asymmetry, which *a priori* may be larger or smaller than that in the current region. Moreover, it is natural to expect that the flavor structure, or more generally the charge, of the target remnant is correlated with the flavor of the struck quark. This expectation has been confirmed experimentally in DIS [47] by the observation of net charge for hadrons (predominantly pions) in the backward region, at $10 < W < 20\ GeV$. Surprisingly, the hadronic net charge in the backward region is observed to be even *larger* than that in the forward region and is found to depend weakly, if at all, on x_{Bj} over the entire measured range $0.01 < x_{Bj} < 0.6$. This is contrary to the behavior of net charge in the forward region, which diminishes significantly with decreasing x_{Bj} values. Hence, hadrons (such as the Λ) that are produced largely in the backward region may also be useful for flavor tagging, provided the direct DIS process can be isolated. Since in the forward region, the current correlations are generally large, it is advantageous, from the point of view of flavor tagging, to choose the lowest z-cut that optimizes the sensitivity to desired quark flavors, *irrespective of target contamination.* In the next section, a formalism is introduced that allows one to relate polarized quark distributions to a linear combination of arbitrary semi-inclusive asymmetries.

As has been emphasized above, the existence of target correlations, which are generally non-negligible at HERMES kinematics (see Figure 3-2), is irrelevant in the context of flavor tagging. Nevertheless, it may be useful to estimate the relative size of target correlations experimentally. This allows, for example, to determine the applicability of certain models that are based on a particular fragmentation mode (e.g., pure current or target remnant fragmentation) and hence the applicability of analyses that utilize these models.

The essential idea is to compare the size and kinematical evolution of certain hadronic observables with the behavior that would be expected if the dominant process were single quark fragmentation in vacuum (as in e^+e^- collisions). One possibility is to measure violations of charge-isospin symmetry in the measured fragmentation functions, which would naturally arise for significant target correlations. In general, such an analysis will not be easy, since it requires a comparison of the distributions of various hadrons that are usually detected using different methods. An alternative that is especially viable at HERMES, which has already taken data on several light nuclei, is to fix the hadron type (which minimizes acceptance corrections) and instead vary the target nucleus. Since this procedure effectively varies the structure of the target remnant, a comparison of hadron spectra using several (light) nuclear targets may be used to probe the kinematical dependence of target correlations for the various hadrons of interest, provided that nuclear effects [53] can be kept under control.

3.4 Quark Flavor Purities

3.4.1 Definitions

Although expressions for A^h and the corresponding 'probabilities' D_i ($i = 1, 2, 3$ or f) are well known in the high-energy scattering community, the quantities that arise when the inverse reasoning is applied are generally not in use. When a certain hadron h is produced, we define the *quark flavor purity* P_f^h as the probability that a quark with flavor f was struck in the direct DIS reaction. In parton model language, one may write:

$$P_f^h = \frac{e_f^2\, q_f\, D_f^h}{\sum_{f'} e_{f'}^2\, q_{f'}\, D_{f'}} \tag{3.10}$$

where f' runs over all relevant quark and antiquark flavors. It appears that the quantities P_f^h not only have the physically meaningful interpretation mentioned above, but also are very useful when a spin decomposition of the nucleon is attempted using linear combinations of semi-inclusive asymmetries.

In order to introduce this new quantity, let us start with a simple example. Let us assume we accept only high $x_{Bj} > 0.2$ data and that we only probe the direct DIS process. Then, we can consider the nucleon to consist of u and d valence quarks, and define:

$$P_u^{\pi+} = 4uD_u^{\pi+}/(4uD_u^{\pi+} + dD_d^{\pi+}) \tag{3.11}$$

for a proton target. Analogously, expressions for $P_u^{\pi-}$, $P_d^{\pi+}$ and $P_d^{\pi-}$ can be derived. With these definitions, one can write the expression for the semi-inclusive π^+ asymmetry:

$$A^{\pi^+} = P_u^{\pi^+}\frac{\Delta u}{u} + P_d^{\pi^+}\frac{\Delta d}{d} \tag{3.12}$$

Note, that $\sum_f P_f^h = 1$ holds for any hadron. Together with the similar expression for A^{π^-}, one has a set of two equations with two unknowns $\frac{\Delta u}{u}$ and $\frac{\Delta d}{d}$, which can be solved:

$$\frac{\Delta u}{u} = \frac{A^{\pi^+}P_d^{\pi^-} - A^{\pi^-}P_d^{\pi^+}}{P_u^{\pi^+}P_d^{\pi^-} - P_u^{\pi^-}P_d^{\pi^+}} \tag{3.13}$$

$$\frac{\Delta d}{d} = \frac{A^{\pi^-}P_u^{\pi^+} - A^{\pi^+}P_d^{\pi^+}}{P_u^{\pi^+}P_d^{\pi^-} - P_u^{\pi^-}P_d^{\pi^+}} \tag{3.14}$$

Hence, it is clear that the purities P_f^h, and not the fragmentation functions D_f^h, are the relevant quantities if one tries to perform a quark spin decomposition from semi-inclusive asymmetry data. Additionally, the accuracy δ with which Δu and Δd can be extracted from data is closely connected to the purities P_f^h of semi-inclusive hadrons:

$$\delta\left(\frac{\Delta u}{u}\right) = \frac{\sqrt{(P_d^{\pi^-}\delta A^{\pi^+})^2 + (P_d^{\pi^+}\delta A^{\pi^-})^2}}{P_u^{\pi^+}P_d^{\pi^-} - P_u^{\pi^-}P_d^{\pi^+}} \tag{3.15}$$

$$\delta\left(\frac{\Delta d}{d}\right) = \frac{\sqrt{(P_u^{\pi+}\delta A^{\pi-})^2 + (P_d^{\pi+}\delta A^{\pi+})^2}}{P_u^{\pi+}P_d^{\pi-} - P_u^{\pi-}P_d^{\pi+}} \tag{3.16}$$

3.4.2 Generalization to Three Flavors

In reality, for each hadron we have (at least) six quark and antiquark flavors to which we can assign a purity P_f^h: $u, \bar{u}, d, \bar{d}, s, \bar{s}$. This leads to a set of six equations and six unknowns $\frac{\Delta q}{q}$. If we adapt a more general nomenclature for the sub- and superscripts of the P_f^h, equation 3.12 and the analogue expression for the π^- can be written conveniently as:

$$\begin{pmatrix} A^{\pi+} \\ A^{\pi-} \end{pmatrix} = \begin{pmatrix} P_u^{\pi+} & P_d^{\pi+} \\ P_u^{\pi-} & P_d^{\pi-} \end{pmatrix} \begin{pmatrix} \Delta u/u \\ \Delta d/d \end{pmatrix} = \begin{pmatrix} P_{11} & P_{12} \\ P_{21} & P_{22} \end{pmatrix} \begin{pmatrix} \Delta u/u \\ \Delta d/d \end{pmatrix} \tag{3.17}$$

This expression can be generalized to six quark and antiquark flavors by defining a 6×6 matrix $\mathcal{P}$ which contains the purities of six hadrons (e.g., at HERMES, one might choose from π^0, π^+, π^-, K^0, K^+, K^-, p, $\bar{p}$).

$$\vec{A} = \mathcal{P}\left(\frac{\overrightarrow{\Delta q}}{q}\right) \tag{3.18}$$

When the matrix elements of $\mathcal{P}$ are determined (from experiment, existing data or simulations), equation 3.18 holds all information needed to extract the quark spin distributions from semi-inclusive spin asymmetries using one specific target. The practicality of this formula can be seen from the trivial way of calculating the uncertainties in $\left(\frac{\Delta q}{q}\right)_i$ from the statistical errors of the measured quantities A_i ($i = 1, 6$):

$$\frac{\overrightarrow{\Delta q}}{q} = \mathcal{P}^{-1}\vec{A} \Longrightarrow \left(\frac{\Delta q}{q}\right)_i = \sum_j (\mathcal{P}^{-1})_{ij} A_j = \sum_j \frac{\det \mathcal{P}_{ji}}{\det \mathcal{P}} A_j \tag{3.19}$$

where $\det \mathcal{P}_{ij}$ is the cofactor of the matrix elements $\mathcal{P}_{ij}$, namely the determinant of the $(N-1) \times (N-1)$ matrix, obtained by omitting the ith row and the jth column, multiplied by $(-1)^{i+j}$ (Cramer's rule). The uncertainties in $\left(\frac{\Delta q}{q}\right)_i$ can then be written:

$$\delta\left(\frac{\Delta q}{q}\right)_i = \frac{\sqrt{\sum_j (\det \mathcal{P}_{ji}\delta A_j)^2}}{\det \mathcal{P}} \tag{3.20}$$

In practice, HERMES might not be able to extract all six asymmetries accurately. The quark flavor purity matrix $\mathcal{P}$ then becomes a matrix with dimensions $N \times N$, where $6 - N$ is the number of 'known' factors $e_f^2 D_f^h \Delta q_f / q_f$ which are introduced by hand into equation 3.18, using data from other experiments or from Monte Carlo simulations.

The presented approach can be used for any number of asymmetries that have to be linearly combined in order to extract information on the quark spin distributions. If, for example, the small contribution from Δs and $\Delta\bar{s}$ is assumed to be known, $\vec{A}$ might have the form:

$$\begin{pmatrix} A_1 - P_s^{\pi^+}\frac{\Delta s}{s} - P_{\bar{s}}^{\pi^+}\frac{\Delta\bar{s}}{\bar{s}} \\ A_2 - P_s^{\pi^-}\frac{\Delta s}{s} - P_{\bar{s}}^{\pi^-}\frac{\Delta\bar{s}}{\bar{s}} \\ A_3 - P_s^{p}\frac{\Delta s}{s} - P_{\bar{s}}^{p}\frac{\Delta\bar{s}}{\bar{s}} \\ A_4 - P_s^{\bar{p}}\frac{\Delta s}{s} - P_{\bar{s}}^{\bar{p}}\frac{\Delta\bar{s}}{\bar{s}} \end{pmatrix} \tag{3.21}$$

Here, A_1 through A_4 were chosen to correspond to the spin asymmetries of semi-inclusive π^+, π^-, protons p and antiprotons $\bar{p}$, respectively.

3.5 A *PEPSI* Simulation of Quark Flavor Purities

3.5.1 Introduction to the Simulations

The deep inelastic scattering cross section for semi-inclusive processes relevant to HERMES has been studied using the Monte Carlo program for polarized leptoproduction *PEPSI* (Version 1.3) [49]. The parton distributions chosen were those from Gehrmann *et al.* [54], corresponding to set 110 in *PEPSI*. The LUND string fragmentation model was chosen to handle the fragmentation of the quarks into hadrons. The standard fragmentation parameters in *PEPSI* were used (not fitted to HERMES data).

Events were generated for an electron beam energy of 27.56 GeV, requiring the following DIS cuts on the kinematic variables of the electron: $Q^2 > 1$ (GeV/c)^2, $W^2 > 4$ GeV^2, $y < 0.85$. The full x_{Bj} region was accepted in the simulations. The HERMES geometrical acceptance was approximated by a box ($|\theta_x| < 120$ $mrad$ and $40 < |\theta_y| < 140$ $mrad$), complemented by the following requirements:

- particles with momenta less than 800 MeV are not detected; and
- the θ_x behavior of particles with momenta between 0.8 and 2.5 GeV was considered in detail for positively and negatively charged particles separately, to take into account the influence of the dipole magnet field on relatively slow particles.

We have investigated the purities P_f^h for all relevant hadrons and for all six quark and antiquark flavors as a function of x_{Bj} and z. A free neutron target was chosen and nuclear corrections have not been taken into account. This was done since it is generally assumed that the experimental ^{3}He asymmetry will essentially be formed by hadrons that fragment from a quark which resided in the neutron before the scattering reaction took place. As a comparison, we also show the quark flavor purities for charged pions, kaons and protons coming from a proton target. The results of the simulations are in good agreement with expectations from quark counting rules and established parameterisations for the fragmentation functions.

3.5.2 Results from the Simulations

An overview of all results can be found in the Appendix in the form of plots. Note that the quark flavor nomenclature used in the plots and in the forthcoming sections is target dependent. Thus, when talking about results for a neutron (proton) target, we intentionally write $q_f(x)$ for the distribution of the f quark in the neutron (proton). They may, of course, be related to one another by assuming isospin symmetry.

The following results have been obtained using a ${}^1_0n$ target in *PEPSI*. The general conclusions, however, are also valid for a proton target (and, consequently, for any nuclear target).

- It was found that the $\pi^+(=u\bar{d})$ is a very good probe for the u-quark, due to the factor $\frac{4}{9}$ which stems from e_u^2. For $z > 0.1$ and $x_{Bj} > 0.1$, about 75 % of all π^+ are produced in reactions off a u-quark. For higher z-cuts the purity increases to values above 85 %. The purity of π^+ coming from a $\bar{d}$-quark, $P_{\bar{d}}^{\pi+}$, is typically between 5 and 10 %, which essentially tells one that the π^+ asymmetry can not be used for the extraction of $\Delta\bar{d}$.

- The purity of $\pi^-(=\bar{u}d)$ coming from d-quarks, $P_d^{\pi-}$, is drastically lower than its charge conjugate $P_u^{\pi+}$, mainly due to the low charge of the d-quark ($e_d^2 = \frac{1}{9}$). For $x_{Bj} > 0.1$, $P_d^{\pi-} = 40 - 70$ %, for $z > 0.1...0.6$. A large fraction of π^- stem from reactions off either u-quarks (due to charge and abundance) or $\bar{u}$ quarks (due to charge and due to the fact that there is a valence $\bar{u}$-quark in the π^-). Below $x_{Bj} = 0.06$, $P_{\bar{u}}^{\pi-}$ is larger than $P_d^{\pi-}$, saturating at its maximum value of 40 % at low x_{Bj}. A π^--asymmetry will essentially probe a combination of Δu, Δd, and $\Delta\bar{u}$.

- P_u^{K+}, the u-quark purity for the K^+ $(= u\bar{s})$, essentially behaves like $P_u^{\pi+}$, which is not surprising. In the valence region, $70 - 80$ % of the K^+ are produced in reactions off a u-quark, while at the lowest attainable x_{Bj} it decreases to 60 %. The $\bar{s}$-quark is responsible for about 10 % of the K^+ over the full x_{Bj} range.

- Usually, the K^- is considered an exquisite probe in semi-inclusive physics, because it is an 'all-sea-object'. In the simulations we indeed find a large sensitivity to sea quarks. Trivially, due to its charge the $\bar{u}$-quark has the largest purity – up to 60 % for $z > 0.6$ and $x_{Bj} \simeq 0.1$. The sensitivity to the s-quark is about $10 - 15$ %. The rest of the purity is essentially taken up by the u-quark.

- The K_S^0 might be considered interesting because of its sensitivity to the strange quark sea. However, we find that $P_{s+\bar{s}}$ for the K_S^0 does not exceed 25 % in any region in x_{Bj} up to cuts as high as $z > 0.6$. On the contrary, about half of the ϕ mesons come from s or $\bar{s}$ quarks in the nucleon. Unfortunately, it will be difficult to isolate the ϕ mesons produced in direct DIS from the overwhelming amount produced in resolved processes.

As an example, the purity matrix P has been constructed for pion and kaon asymmetries at $x_{Bj} = 0.1$, integrated over $z > 0.4$.

$$\begin{pmatrix} A^{\pi^+} \\ A^{\pi^0} \\ A^{\pi^-} \\ A^{K^+} \\ A^{K^0} \\ A^{K^-} \end{pmatrix} = \mathcal{P}\ \frac{\overrightarrow{\Delta q}}{q} = \begin{pmatrix} 0.75 & 0.10 & 0.00 & 0.07 & 0.08 & 0.00 \\ 0.48 & 0.28 & 0.00 & 0.17 & 0.07 & 0.00 \\ 0.27 & 0.42 & 0.00 & 0.27 & 0.05 & 0.00 \\ 0.72 & 0.14 & 0.00 & 0.02 & 0.01 & 0.07 \\ 0.14 & 0.67 & 0.00 & 0.08 & 0.03 & 0.08 \\ 0.18 & 0.11 & 0.12 & 0.48 & 0.07 & 0.02 \end{pmatrix} \begin{pmatrix} \Delta u/u \\ \Delta d/d \\ \Delta s/s \\ \Delta \bar{u}/\bar{u} \\ \Delta \bar{d}/\bar{d} \\ \Delta \bar{s}/\bar{s} \end{pmatrix} \tag{3.22}$$

Inverting the complete 6×6 matrix above yields expressions for the $\Delta q/q$ that generally consist of five or six terms with large numbers that partially cancel in the sum over asymmetries. One immediately recognizes the important contribution of asymmetries that are prone to large uncertainties due to low statistics. In this example, the A^{π^0} term causes particular concern.

Thus, the uncertainties need to be optimized separately for different kinematical regions. Several methods of optimization are available:

- Neglect small purities, e.g., smaller than 0.1. This leads to a matrix of fewer dimensions, and consequently to the need for a smaller number of significant semi-inclusive asymmetries. In this way, the asymmetries with high purities can be selected for the calculation.

- Select the most favorable asymmetries. The choice made above is arbitrary, although at HERMES we can not choose from a large number of independent asymmetries. We, however, expect that a combined $K^+ + p$ asymmetry will be largely sensitive to the u quark. The charge-isospin conjugate case is also expected to be true, although to a somewhat lesser extent.

- Choose independent asymmetries and optimize statistics by selecting different kinematical regions. A natural choice for two of the asymmetries would be positively and negatively charged hadrons. However, none of the other possible asymmetries will be independent, since all available data are included in the former two. In the 1995 data, one can solve this problem by choosing only hadrons with momenta p smaller than 6 GeV/c. This leads to an asymmetry vector $\vec{A} = (A^{h^+(p<6)}, A^{h^-(p<6)}, A^{\pi^+}, A^{\pi^-}, A^{K,p^+}, A^{K,p^-})$.

Chapter 4

The Transversity Distribution h_1

4.1 Introduction

Although much attention has been focused on the measurement of quark helicity distributions in the nucleon, the role of transverse polarization in deep inelastic scattering has been largely ignored. On the other hand, within perturbative QCD, transverse and longitudinal spin effects are on a completely equal footing [55]. Hence, the study of transverse spin effects should be viewed as an integral part of the spin program in DIS. In addition, the importance of transverse polarization in inclusive hadron production in high-energy hadronic reactions [56] may indicate that many surprises await us [57] in the study of semi-inclusive DIS on transversely polarized targets.

The subsequent sections describe the possibility of a measurement at HERMES of the chiral-odd structure function $h_1 = \frac{1}{2}\sum_f e_f^2\, \Delta_\perp q_f$ [58, 55, 59, 19]. Together with the spin-averaged q_f and helicity Δq_f quark distributions, the transversity distributions $\Delta_\perp q_f$ completely specify the quark state in the nucleon at the leading twist-two level. The physics motivation for such a measurement, particularly a possible sensitivity to Δg, is discussed in some depth.

4.2 Physics Motivation

4.2.1 Quark Distribution Functions

It can be understood [55] why exactly three quark distributions, one spin-averaged and two spin-dependent, are necessary to describe the hard scattering process at leading twist (or, more generally, any higher twist) by enumerating the independent helicity amplitudes $\mathcal{F}_{hh',HH'}$, where h, h' and H, H' are quark and nucleon helicities, respectively. Using helicity conservation ($h + H = h' + H'$), together with invariance under parity ($\mathcal{F}_{hh',HH'} = \mathcal{F}_{-h-h',-H-H'}$) and time reversal ($\mathcal{F}_{hh',HH'} = \mathcal{F}_{h'h,H'H}$), it is straightforward to show that only three independent amplitudes remain:

$$\begin{aligned} \mathcal{F}_{+\frac{1}{2}+\frac{1}{2},+\frac{1}{2}+\frac{1}{2}} &= q + \Delta q \\ \mathcal{F}_{+\frac{1}{2}+\frac{1}{2},-\frac{1}{2}-\frac{1}{2}} &= q - \Delta q \\ \mathcal{F}_{+\frac{1}{2}-\frac{1}{2},-\frac{1}{2}+\frac{1}{2}} &= \Delta_\perp q \end{aligned} \tag{4.1}$$

It is clear that q is independent of spin, Δq measures a helicity difference, and $\Delta_\perp q$ involves a helicity (*and* chirality) flip.

A perhaps more physical argument may be given as follows [60]. Consider a nucleon that is moving in the $\hat{z}$ direction with its polarization in the $\hat{x}$ direction. At twist-two, which is the only contribution that survives in the formal DIS limit $Q^2, \nu \to \infty$ (x_{Bj} fixed), the nucleon may be viewed as a beam of collinear and non-interacting partons. Then, the quark eigenstates at twist-two are exactly those that characterize a free quark, namely the momentum p_z, the helicity $|z\pm\rangle$ (angular momentum about $\hat{z}$), and the transversity (eigenstate of transversely projected Pauli-Lubanski operator) $|x\pm\rangle = \sqrt{\frac{1}{2}}\,[\,|z+\rangle \pm |z-\rangle\,]$.

It should be stressed that [59] h_1 does *not* measure the quark's transverse spin distribution, since essentially $[S_x, p_z] \neq 0$. (The average transverse spin $\langle S_x\rangle = g_T \equiv g_1 + g_2$ is a twist-3 structure function, involving quark-gluon correlations.) However, in the non-relativistic limit, transversely polarized quarks are in transverse spin eigenstates [60], so that rotational invariance implies:

$$\Delta_\perp q = \Delta q \tag{4.2}$$

Thus, the splitting between $\Delta_\perp q$ and Δq, which are in general independent distributions, is completely removed in the limit that quarks are non-relativistic. It is then clear that *the difference between $\Delta_\perp q$ and Δq is sensitive to the role of relativistic effects in the nucleon state.*

4.2.2 Adding Gluons

The reasoning that leads to the above conclusion takes into account quark degrees of freedom only. On the other hand, there are good reasons to believe that polarized gluons contribute at *leading order* to the measured parton helicity distributions in a nucleon. Adopting this point of view, it is shown below that an appropriate comparison of the longitudinal and transverse structure functions may be used to probe the gluon polarization in a nucleon.

There has been much controversy in the literature over the anomalous polarized gluon contribution to the quark singlet axial charges [61, 62, 63, 64]. Rather than considering the details of the different points of view, we present the consequences of one particular approach [15, 61, 62, 63] that has several attractive features. On the other hand, some authors [65, 66] suggest that the issue of whether or not polarized gluons contribute to g_1 depends entirely on the factorization scheme chosen. That may also be an acceptable view: different schemes correspond to various interpretations of the measured structure functions, a situation that is not uncommon in QCD physics. At the very least, it is safe to say that polarized gluons *can* contribute to g_1. Then, the measurements considered below may be useful in understanding the connection between spin structure functions and dynamical models of nucleon spin structure in terms of quark and gluon degrees of freedom.

The matrix elements of quark axial currents have the interesting property that they receive important contributions from around the ultraviolet cutoff scale $k_\perp^2 \sim$

Q^2 [15, 67]. On the other hand, the degrees of freedom that we ordinarily associate with those of the nucleon correspond to low-lying states around the confinement scale $k_\perp^2 \sim \Lambda_{QCD}^2$. It has been shown that [15] factorization of the cross section into a soft part and a hard part beyond the leading order unambiguously defines the gauge invariant quark and gluon helicity distributions in the nucleon that contribute to the first moment of g_1. These distributions are unique and scheme independent provided that the helicity structure of the theory is preserved at tree level and that the current quark masses are negligibly small (or very large) compared to the hadronic scale Λ_{QCD}. In the soft part, gluons do not appear as explicit partonic degrees of freedom. Hence, for light quark flavors, this part can be physically interpreted as scattering off sea quarks.

If one adopts this point of view, it is straightforward to identify the first moments of the polarized structure functions:

$$\begin{aligned} \int g_1(x_{Bj}, Q^2) dx_{Bj} &= \frac{1}{2} \sum_f e_f^2 \left(\Delta q_f(Q^2) - \frac{\alpha_s}{2\pi} \Delta g(Q^2) \right) \\ \int h_1(x_{Bj}, Q^2) dx_{Bj} &= \frac{1}{2} \sum_f e_f^2 \Delta_\perp q_f(Q^2) \end{aligned} \tag{4.3}$$

It is important to note that, due to angular momentum conservation, independent of scheme and gauge, there is no gluon helicity flip distribution at leading twist that could mix with $\Delta_\perp q$, contrary to the case with Δq and Δg. That is, there are only two gluon helicity amplitudes at leading twist:

$$\begin{aligned} \mathcal{F}_{+1+1,+\frac{1}{2}+\frac{1}{2}} &= g + \Delta g \\ \mathcal{F}_{+1+1,-\frac{1}{2}-\frac{1}{2}} &= g - \Delta g \end{aligned} \tag{4.4}$$

Hence, together with the previous considerations, it can be concluded that a comparison of the (C-even) structure functions h_1 and g_1 gives information about both the size of relativistic effects *and* the value of Δg.

Although relativistic effects are not well known, aside from model or sum rule estimates [55, 59], they may be experimentally measured in semi-inclusive processes.

Since gluon observables are $C+$ objects, $\Delta_\perp q_f^-$ and Δq_f^- are both free of the gluon anomaly, where $\Delta_{(\perp)} q_f^-$ is defined to be the $C-$ helicity (transversity) distribution. Hence, independent of any gluon contributions, the size of relativistic effects (in $C-$ observables) can be determined directly by comparing measurements of $\Delta_\perp q_f^-$ and Δq_f^-. Assuming that relativistic effects are equal for both $C-$ and $C+$ quark distributions, the first moment of the gluon helicity distribution, $\Delta g(Q^2)$, can be probed via the following observable, at leading order:

$$\Delta g(Q^2) \simeq \frac{2\pi}{\alpha_s(Q^2)} \left[\frac{\Delta q^-(Q^2)}{\Delta_\perp q^-(Q^2)} \cdot \Delta_\perp q(Q^2) - \Delta q(Q^2) \right] \tag{4.5}$$

This idea is similar in spirit to one already proposed in [68] to compare g_1 with the C-odd spin structure function g_3, measurable in inclusive neutrino scattering off a polarized nucleon. Ideas to probe the gluon anomaly by comparing inclusive and semi-inclusive observables in DIS have also been previously discussed in [69, 70].

An unambiguous identification of the hard part is not generally possible for moments higher than the first [15], since the polarized gluon splitting function (that couples to $\Delta g(Q^2)$) is regularization scheme dependent. However, one may argue that it is a natural choice to compare Δq with $\Delta_\perp q$ (in terms of soft quark degrees of freedom) using the particular scheme in which the former is conserved. In that case, higher moments of $\Delta g(Q^2)$, and hence [71] its dependence on momentum fraction x_{Bj}, can be extracted in a completely analogous way, provided that radiative corrections do not spoil the factorisation of scales observed at leading order [15, 72].

4.3 Measuring h_1

The h_1 structure function has not yet been measured. Since h_1 is chiral-odd, it decouples from *inclusive* hard scattering because perturbative QCD preserves chirality modulo quark mass corrections, which are negligibly small for light quark flavors [73]. On the other hand, h_1 can enter into semi-inclusive reactions, such as polarized Drell-Yan [58, 59, 55] or semi-inclusive deep inelastic scattering [73, 19] on transversely polarized nucleons. The former measurement can be done at RHIC and has already been proposed by the RHIC Spin Collaboration [74]. Several methods are available for measuring h_1 in semi-inclusive DIS. The simplest one experimentally, since it requires only one hadron in the final state whose spin need not be measured, has been discussed in [73]. It uses the fact that h_1 can couple to a chiral-odd fragmentation function, thereby preserving quark chirality. Since the polarization of the struck quark is not measured, the single-hadron asymmetry appears only at the twist-3 level, and is thus suppressed as $\frac{1}{Q}$: the twist-3 distribution function g_T couples to the usual twist-2, chiral-even fragmentation function D, and h_1 couples to a twist-3, chiral-odd fragmentation function E (usually written $\hat{e}_1$ in the literature). Despite the $\frac{1}{Q}$ kinematical suppression of the asymmetry, such a measurement is particularly feasible at HERMES, as shown in the remainder of this Chapter.

For completeness, other methods proposed to measure the nucleon's transversity distribution in semi-inclusive DIS are briefly mentioned. It is possible to measure h_1 at *leading twist* by analyzing the transverse polarization of the struck quark. One approach is to measure the (vector) polarization of a leading hadron, such as that of the Λ [19, 20, 21] via the angular decay distribution in its dominant non-leptonic decay $\Lambda \to p\pi$. Then, in principle, the Λ polarization can couple to that of a current quark. The size of this spin correlation and its dependence on the flavor of the current quark are not known. If such a correlation exists, it is presumably sensitive to how the spin (or transversity) of the Λ is distributed among its quark flavors. It may be estimated from a measurement of the Λ polarization in semi-inclusive DIS using a longitudinally polarized beam incident on an unpolarized target [20]. Regarding such measurements, it is worth mentioning that hyperons, especially the Λ, produced in fixed target proton-proton and proton-nucleus collisions exhibit large polarization values, even though neither beam nor target are polarized [75, 76, 77]. Another approach to measuring the quark's transverse polarization is via the Collins effect [22]: since the fragmentation of a transversely polarized quark is *a priori* not invariant under rotation about the quark momentum, this may lead to an azimuthal asymmetry in hadron production. Such an effect clearly depends on final state interactions, which are unknown and may be small. Although these measurement are not considered below, it is important to search for spin-dependent effects in fragmentation. They are not only useful for probing the nucleon's polarized quark distributions, but also interesting in their own right.

4.3.1 Calculation of the Asymmetry

The spin-dependent part of the cross section for semi-inclusive DIS of hadrons h with longitudinally polarized beam on a transversely polarized target is given by [73]:

$$\frac{d^4\Delta\sigma^h}{dx_{Bj}\,dy\,dz\,d\phi} = \frac{4\alpha^2}{Q^2}\,\cos\phi\,\gamma\sqrt{1-y}\left[H_2^h - H_1^h(1-\frac{y}{2})\right] \tag{4.6}$$

where ϕ is the angle between the polarization plane (defined by polarizations of beam and target) and the scattering plane (defined by momenta of incident and scattered leptons), and[1]

$$H_1^h = \frac{1}{2}\sum_f e_f^2\,\Delta q_f\,D_f^h \tag{4.7}$$
$$H_2^h = \frac{1}{2}\sum_f e_f^2\,[\Delta_T q_f D_f^h + \frac{\Delta_\perp q_f}{x_{Bj}}\frac{E_f^h}{z}]$$

Here, $\Delta_T q_f$ refers to the quark flavor contribution to g_T, and should not be confused with $\Delta_\perp q_f$, which is used to denote the quark flavor contribution to h_1. The factor $\gamma \equiv \frac{\sqrt{Q^2}}{\nu} = \frac{2M_N x_{Bj}}{\sqrt{Q^2}}$ in the asymmetry explicity indicates that it is a twist-three effect (i.e., leading $\frac{1}{Q}$ behavior at fixed Bjorken x_{Bj}). The presence of the helicity distribution dependent term H_1^h, usually associated with a longitudinally polarized target, occurs because of a finite longitudinal polarization of the nucleon relative to the direction of the virtual photon (in the nucleon's rest frame).

It can be seen directly from eqn. 4.7 that the term containing contributions from h_1 is enhanced relative to the other terms by $\frac{1}{x_{Bj}}$, which is essentially due to the chiral-odd nature of h_1. Hence, in the limit of small x_{Bj}, the asymmetry becomes completely

[1] Note that gluon observables are not explicitly written in the subsequent formulae; they may be introduced easily by using eqn. 4.3.

dominated by its contribution from h_1 (multiplied, of course, by the unknown chiral-odd fragmentation function E). Since both $\Delta_\perp q_f$ and E_f^h are unknown, except for a few simple model estimates, it is *a priori* difficult to extract information about either of them, except perhaps to confirm that they are non-zero. However, the chiral-odd fragmentation functions at leading twist are distinguished from the usual (chiral-even) fragmentation functions only by coherent gluon radiation [73], which is flavor independent and should thus preserve the flavor correlations observed in unpolarized semi-inclusive DIS; hence, the flavor tagging methods introduced in Chapter 3 can be used accordingly.

As a particular example, consider the single-pion charge difference asymmetry:

$$A = \frac{N_{\uparrow\rightarrow}^{\pi^+-\pi^-} - N_{\uparrow\leftarrow}^{\pi^+-\pi^-}}{N_{\uparrow\rightarrow}^{\pi^+-\pi^-} + N_{\uparrow\leftarrow}^{\pi^+-\pi^-}} \tag{4.8}$$

Since the measurement integrates over the transverse momenta $\vec{p_t}$ of the pions, we expect that the fragmentation functions are independent of the polarization state of the struck quark at leading order (see Chapter 3). In addition, invariance under charge and isospin conjugation reduces the number of independent functions to three (for light quark fragmentation into pions):

$$\begin{aligned} D_1 &= D_u^{\pi^+} = D_{\bar{d}}^{\pi^+} = D_d^{\pi^-} = D_{\bar{u}}^{\pi^-} \\ D_2 &= D_u^{\pi^-} = D_{\bar{d}}^{\pi^-} = D_d^{\pi^+} = D_{\bar{u}}^{\pi^+} \\ D_3 &= D_s^{\pi^-} = D_{\bar{s}}^{\pi^-} = D_s^{\pi^+} = D_{\bar{s}}^{\pi^+} \end{aligned} \tag{4.9}$$

and likewise for the chiral-odd fragmentation functions E. Unfortunately, contrary to case with a longitudinally polarized target, these assumptions alone are not sufficient to obtain an asymmetry that depends on distribution functions only. It is also necessary to specify the ratio:

$$\frac{1}{z}\frac{E_1 - E_2}{D_1 - D_2} \tag{4.10}$$

Ji [78] has recently calculated fragmentation functions for u quarks into charged pions (D_1 and D_2) in lowest order of chiral quark theory. The results are in good agreement with data [79]. For the chiral-odd fragmentation function at leading twist, he finds:

$$\frac{E}{z} = \frac{m_q}{M} D \simeq \frac{D}{3} \tag{4.11}$$

where $m_q \sim \frac{M}{3}$ is taken to be the constituent quark mass. This simple relation can be physically understood by recalling that the two fragmentation functions differ by a chirality flip, which is here accomplished via a (constituent quark) mass insertion.

Using eqn. 4.11 and assuming that the strange sea is charge conjugation even yields (for a proton target):

$$\frac{1}{x_{Bj}} \cdot \frac{A^p}{D\ p_T\ p_B} = \cos\phi\ \left(\frac{M_N}{\sqrt{Q^2}}\right) \left[\frac{4\sqrt{1-y}}{y + \frac{2(1-y)(1+R)}{y}}\right] \cdot$$

$$\left\{\frac{4\left[\frac{\Delta_\perp u^-}{3\, x_{Bj}} + \Delta_T u^- - (1-\frac{y}{2})\Delta u^-\right] - \left[\frac{\Delta_\perp d^-}{3\, x_{Bj}} + \Delta_T d^- - (1-\frac{y}{2})\Delta d^-\right]}{4u^- - d^-}\right\} \tag{4.12}$$

where $p_{T(B)}$ is the polarization of the target (beam), the depolarization factor D takes into account non-unity polarization transfer to the virtual photon at the leptonic vertex, and $R = \frac{\sigma_L}{\sigma_T}$ is the ratio of longitudinal and transverse cross sections. The analogous expressions for other targets may be obtained easily by assuming isospin symmetry for the distribution functions and ignoring nuclear effects to the scattering process. Recent measurements at SLAC on transversely polarized proton and deuteron targets have shown that [80] the twist-3 part of g_2 is consistent with zero, with large error bars. Since no other information is experimentally available, we will ignore any twist-3 contributions to g_2 and use the twist-2 relation [81]:

$$g_2^{tw.-2}(x_{Bj}, Q^2) \quad = \quad -g_1(x_{Bj}) + \int_{x_{Bj}}^1 d\xi\ \frac{g_1(\xi, Q^2)}{\xi} \tag{4.13}$$

which holds for all quark and antiquark flavors. This uncertainty has a very small effect on the asymmetry, since it is suppressed by x_{Bj} relative to contributions from h_1.

4.3.2 Simulation for HERMES

This section provides an estimate of the statistical accuracy with which HERMES can measure the charge difference asymmetries (see eqn. 4.8) on targets of hydrogen, deuterium, and ^3He. Systematic errors, particularly associated with any misalignment of the target field from the pure transverse direction, are not discussed here. Losses of statistics due to reconstruction and particle identification inefficiencies are also not considered.

For asymmetries such smaller than unity, the statistical errors may be calculated from *spin-averaged* counting rates for charged pions:

$$\delta A \simeq \frac{\sqrt{N^{\pi^+} + N^{\pi^-}}}{N^{\pi^+} - N^{\pi^-}} \tag{4.14}$$

To estimate the expected counting rates at HERMES, a PEPSI simulation has been performed as described in Section 3.5.1. Figures 4.1-3 show the estimated statistical accuracy for two standard HERMES runs, assuming the beam and target conditions described in [82]. The solid lines are calculated based on the non-relativistic expectation $\Delta_\perp q_f^- = \Delta q_f^-$, using published parameterizations of parton distributions [83]. The dashed lines correspond to $\Delta_\perp q_f^- = 0$ and illustrate that the asymmetries are dominated by contributions from $\Delta_\perp q_f^-$ at sufficiently small values of x_{Bj}. Without large increases in luminosity (or beam and target polarizations), only measurements on the *proton* appear to be capable of providing the x_{Bj}-dependence of these asymmetries, and hence of h_1. This conclusion results primarily from the assumption that the asymmetry is expected to be significantly larger for the proton than for the neutron.

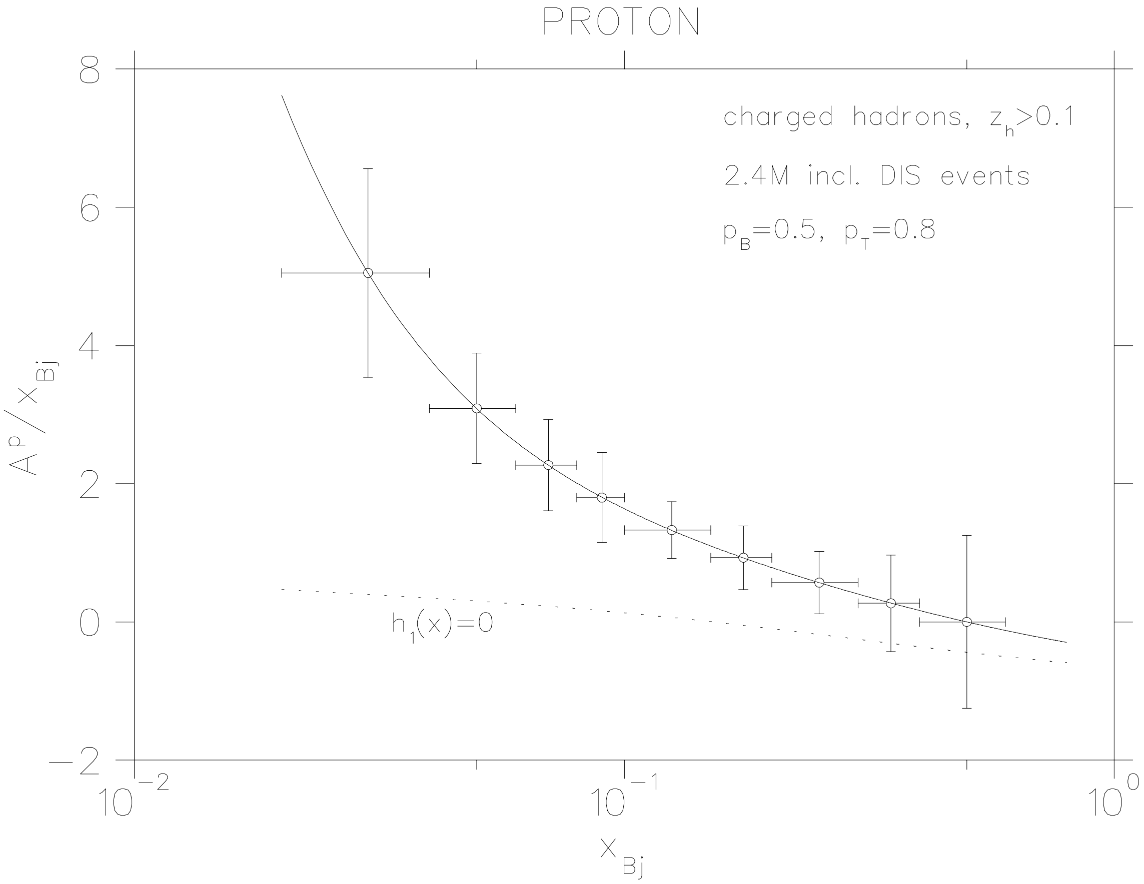

Figure 4-1: The pion charge difference asymmetry for a transversely polarized *proton* target is shown using $\Delta_\perp q_f = \Delta q_f$ (solid line) and $\Delta_\perp q_f = 0$ (dashed line). The error bars indicate the estimated statistical accuracy for two standard HERMES runs, using all charged hadrons with $z_h > 0.1$.

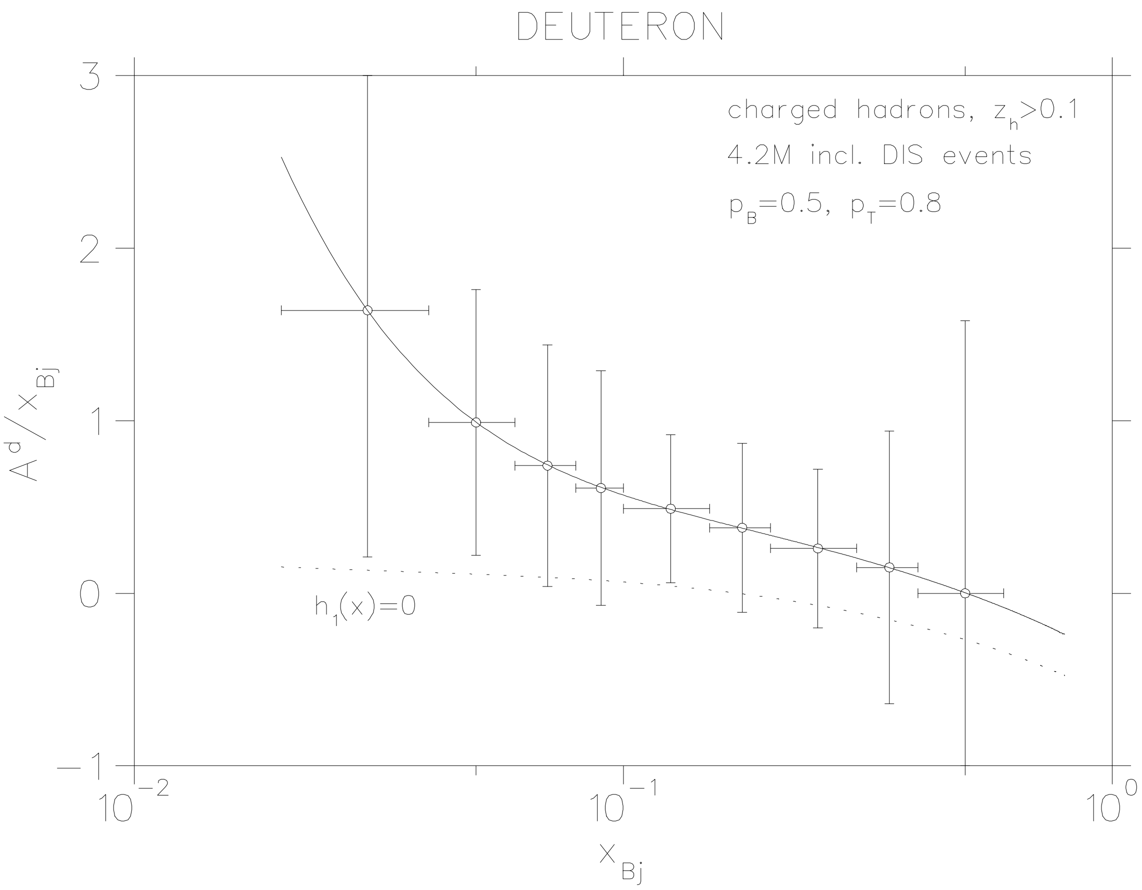

Figure 4-2: The pion charge difference asymmetry for a transversely polarized *deuteron* target is shown using $\Delta_\perp q_f = \Delta q_f$ (solid line) and $\Delta_\perp q_f = 0$ (dashed line). The error bars indicate the estimated statistical accuracy for two standard HERMES runs, using all charged hadrons with $z_h > 0.1$.

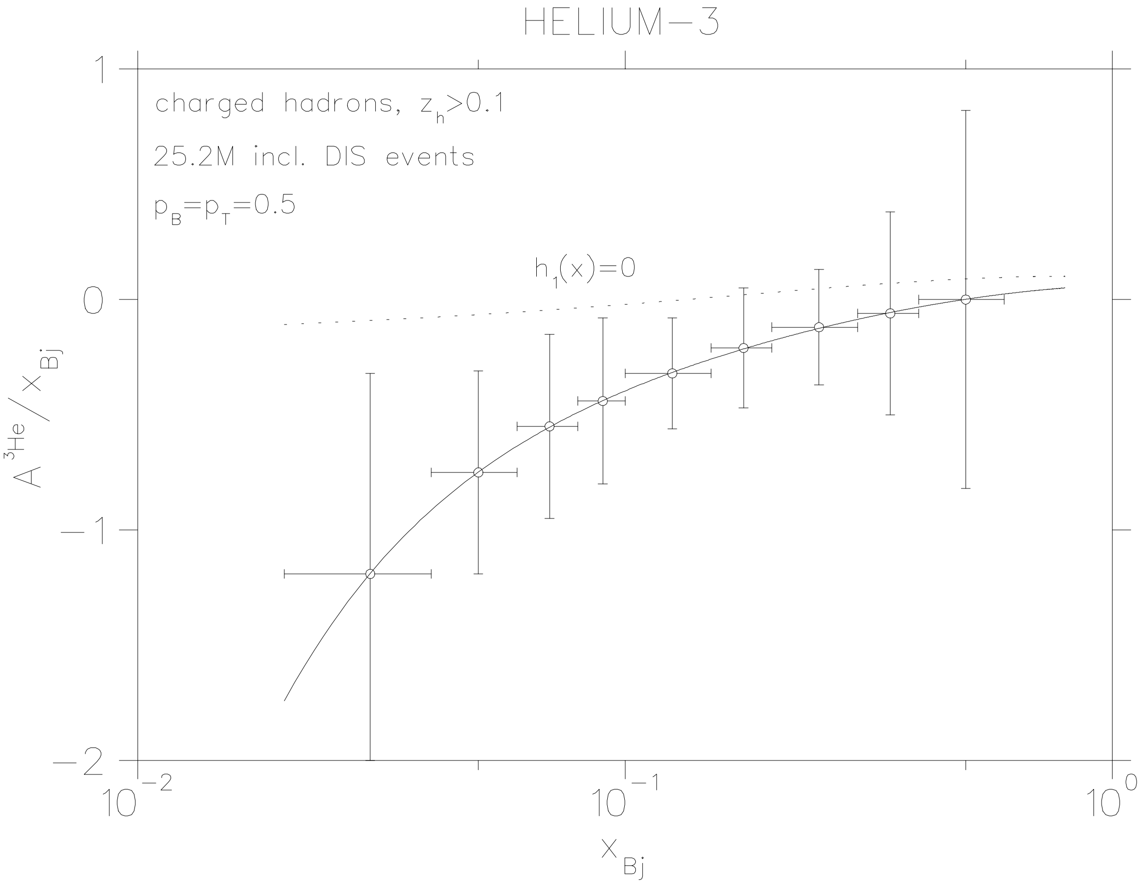

Figure 4-3: The pion charge difference asymmetry for a transversely polarized ^3He target is shown using $\Delta_\perp q_f = \Delta q_f$ (solid line) and $\Delta_\perp q_f = 0$ (dashed line). The error bars indicate the estimated statistical accuracy for two standard HERMES runs, using all charged hadrons with $z_h > 0.1$.

Chapter 5

Conclusions

Deep inelastic scattering on hadronic targets has had a long and fruitful history, providing interesting information on nucleon structure and playing a crucial role in the development of QCD. For example, the discovery of a substantial uncharged component to parton distributions and the verification of the spin-$\frac{1}{2}$ nature of quarks were early successes. Moreover, a quantitative explanation of the scaling violations observed in parton distributions provided one of the first confirmations of QCD dynamics. Following in this tradition, a vigorous program of spin-dependent deep inelastic scattering has been recently undertaken, motivated largely by surprising results from the EMC experiment at CERN in 1987. Further inclusive measurements on polarized nuclear targets have confirmed the conclusions of the initial measurements and provided substantially better constraints on the parton distributions.

On the other hand, the existing, predominantly inclusive data are not sufficient to understand completely the spin structure of the nucleon. It is clear that more exclusive measurements are required to study the more exotic QCD degrees of freedom that contribute to the nucleon's non-perturbative structure. The ability to identify various hadrons in the final state is one of the key advantages of the HERMES experiment at the HERA storage ring, which took its first data on polarized ^3He in the summer of 1995. Several experimental upgrades are currently under development to further increase the particle identification capabilities at HERMES. The aims of HERMES as a second generation spin physics experiment became particularly feasible by the development of two new experimental technologies: a high energy, longitudinally polarized lepton storage ring and a polarized storage cell gas target. The polarization of the leptons, typically of order 50-60%, is naturally caused by the Sokolov-Ternov effect. Internal gas targets can be polarized to a high degree without significant dilution by unpolarized materials, which substantially reduces systematic errors. High luminosities are achieved by using the novel technique of a storage cell.

A direct determination of the charge and flavor structure of parton distributions, with possible sensitivity to strange quarks, is one important motivation for semi-inclusive measurements at HERMES. Interpreting such measurements in terms of quark and gluon degrees of freedom requires an understanding of the parton-hadron correlations that characterize the fragmentation process. A coherent treatment of the theory and phenomenology of quark flavor tagging using semi-inclusive hadrons was presented in this thesis. As an application of those ideas, a general *quark flavor purity* formalism was introduced that allows one to relate quark spin distributions to an arbitrary combination of semi-inclusive asymmetries. The sensitivities of various semi-inclusive hadrons accessible at HERMES to different quark flavors were calculated using a Monte Carlo simulation program based on the Lund fragmentation model.

For deep inelastic scattering on nucleons, relatively little attention has been focused on physics involving transversely polarized targets. Only *inclusive* measurements of the twist-3 structure function g_2 have been carried out at CERN and SLAC. On the other hand, within the framework of perturbative QCD, transverse and longitudinal polarization phenomena are on a completely equal footing. The physics motivation for a measurement of the nucleon's transversity distribution h_1 is discussed in detail in this thesis. No experimental information is available on this structure function, which is necessary for a complete description of the quark state inside the nucleon at leading twist. It was shown that a measurement of the x_{Bj} dependence of the nucleon's transversity distribution h_1 is feasible at HERMES.

The existing data on polarized structure functions indicate that quark helicity degrees of freedom are insufficient to account for the spin of the nucleon. This has stimulated people to look for other possible contributions, namely from quark orbital angular momentum and gluon polarization. In particular, it has been suggested in the theoretical literature that polarized gluons can contribute at leading order to the measured parton helicity distributions. Based on this idea, a novel method was introduced in this thesis to measure the gluon contribution Δg to the total helicity of the nucleon using a comparison of the twist-2 polarized structure functions g_1 and h_1. Hopefully, this will further stimulate measurements of h_1 at HERMES and elsewhere.

Polarization phenomena in high energy leptoproduction, following in the long tradition of deep inelastic scattering measurements, have continued to stimulate the spin physics community. The successful commissioning of the HERMES experiment, with its ability to probe numerous hadronic observables in the final state, represents new and interesting possibilities in the study of spin-dependent hadronic structure. Given the exciting and productive history, we can look forward to additional key insights and, hopefully, new surprises from this establishment of a new experimental frontier in deep inelastic scattering.

Appendix A

Purities of Semi-Inclusive Hadrons at HERMES

This Appendix contains plots that illustrate the kinematical and target dependence of quark flavor purities for relevant hadrons at HERMES. Details of the simulations used to calculate the purities may be found in Section 3.5.1.

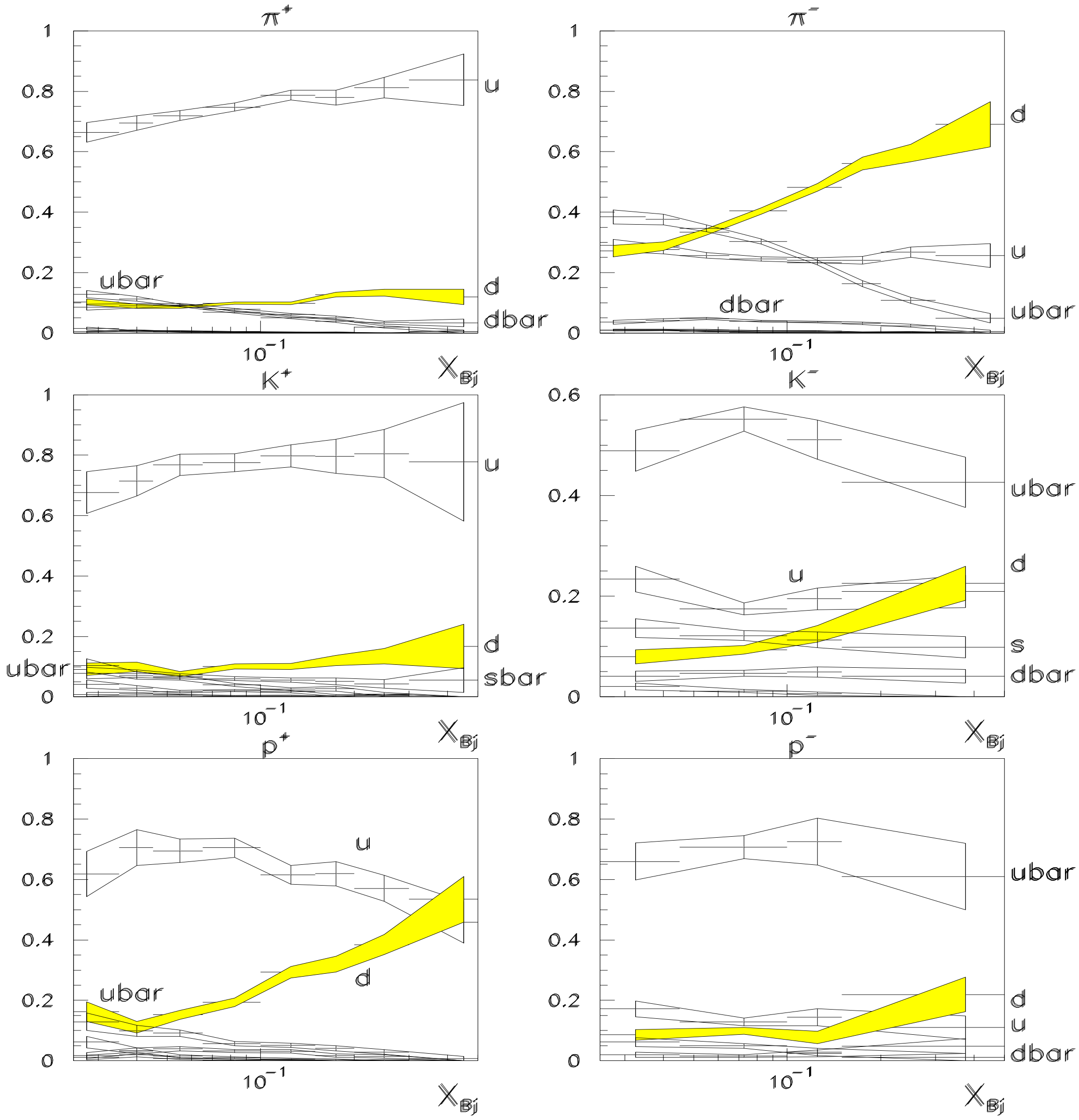

Figure A-1: Purities of the relevant charged hadrons at HERMES as a function of x_{Bj}, for $z > 0.4$ using a neutron target.

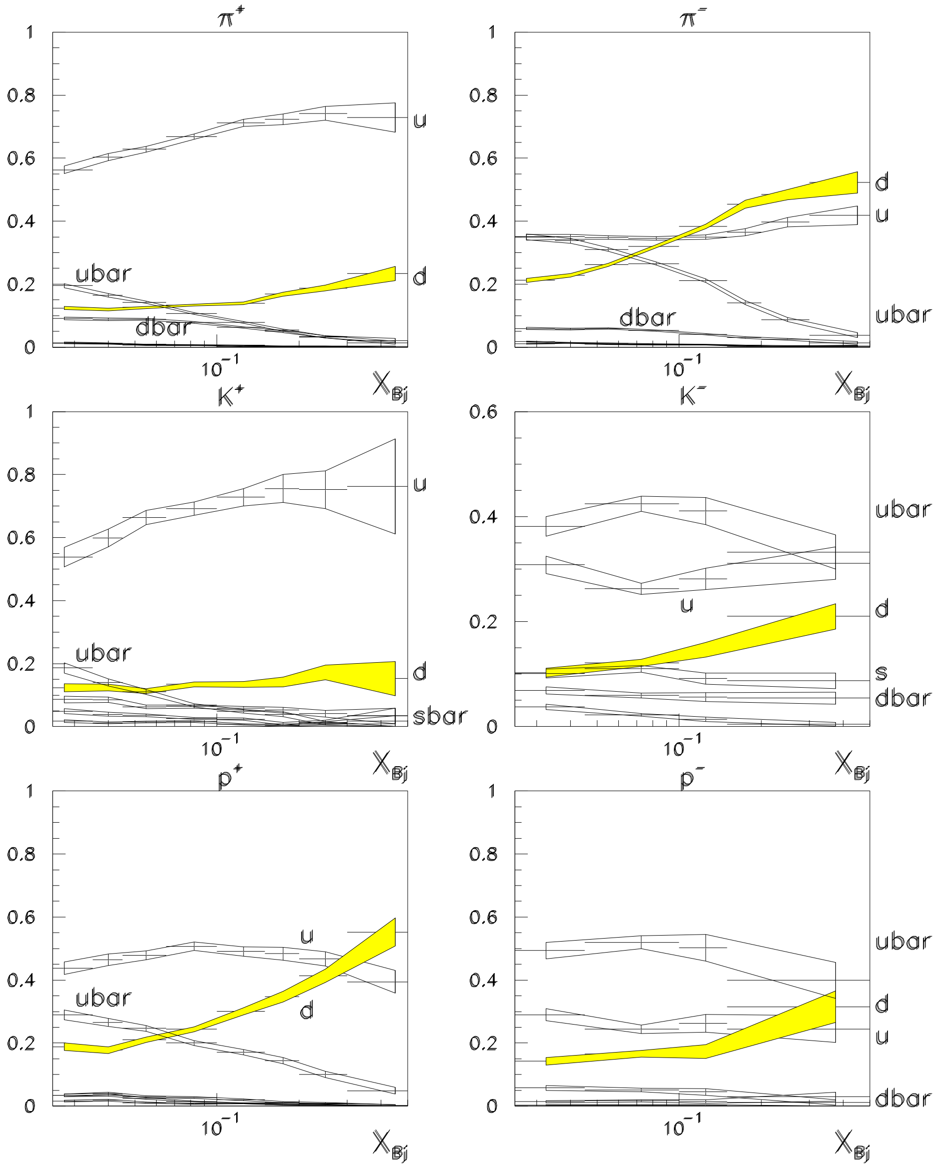

Figure A-2: Purities of the relevant charged hadrons at HERMES as a function of x_{Bj}, for $z > 0.1$ using a neutron target.

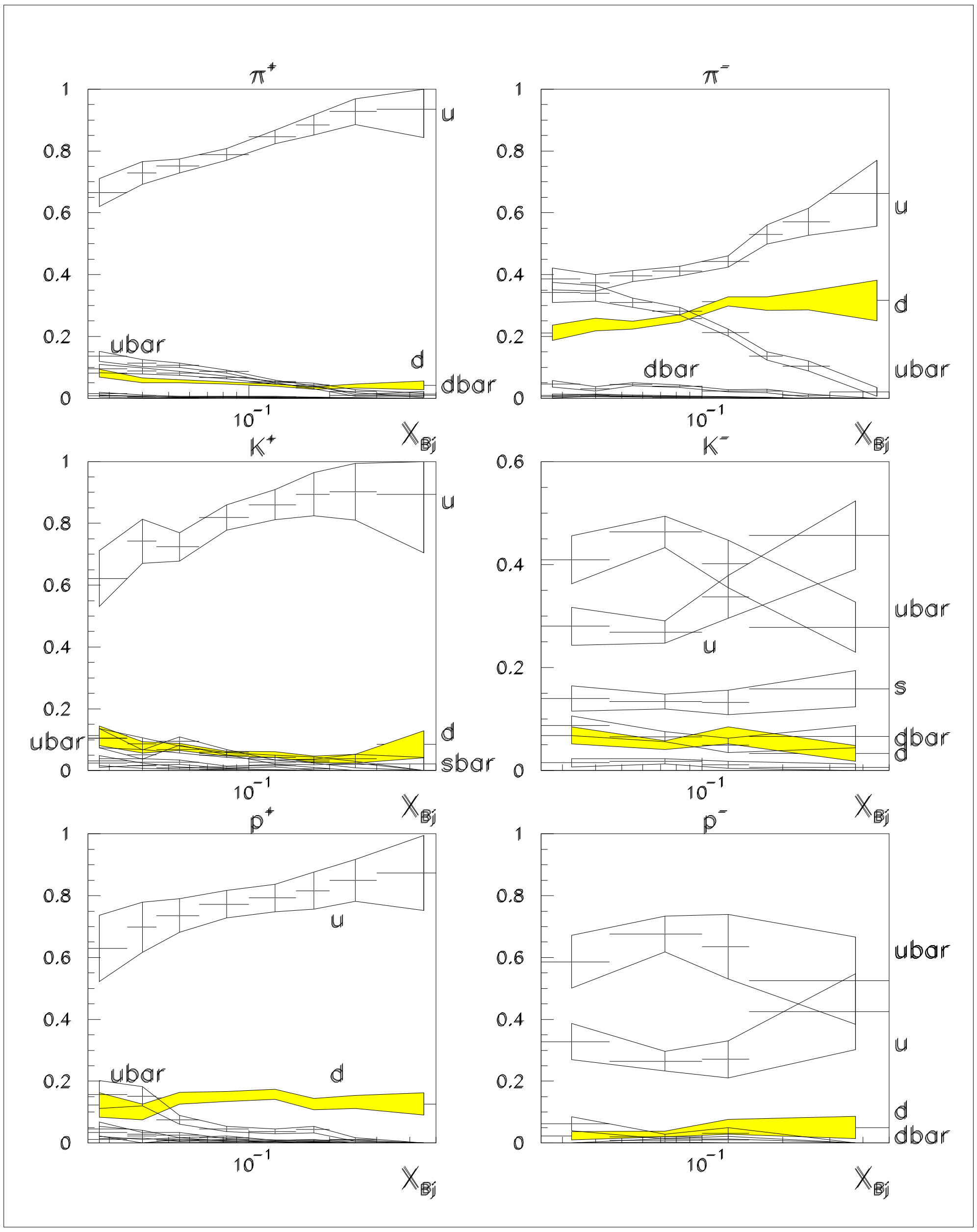

Figure A-3: Purities of the relevant charged hadrons at HERMES as a function of x_{Bj}, for $z > 0.1$ using a proton target.

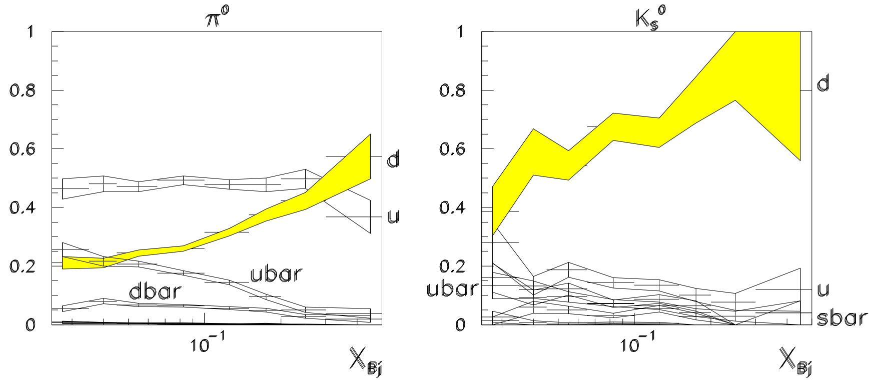

Figure A-4: Purities of the relevant neutral hadrons at HERMES as a function of x_{Bj}, for $z > 0.1$ using a neutron target.

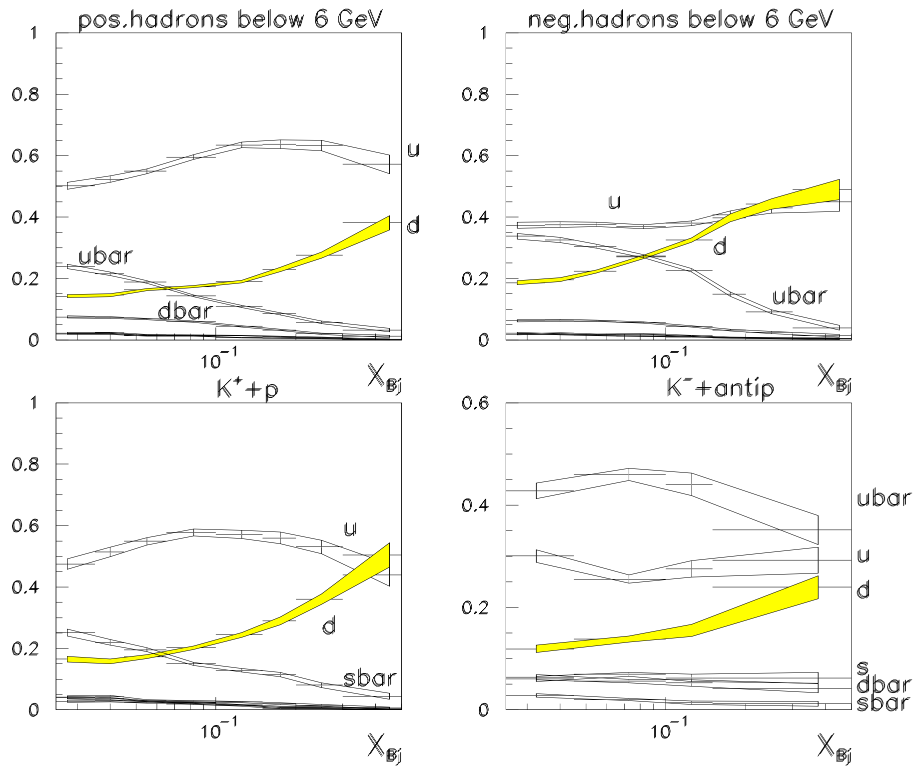

Figure A-5: Purities of charged hadrons below 6 GeV/c, and of the combined kaons and protons above 6 GeV/c at HERMES as a function of x_{Bj}, for $z > 0.1$ using a neutron target.

Bibliography

[1] C. Itzykson and J.B. Zuber, *Quantum Field Theory* (McGraw-Hill, New York, 1980).

[2] J.C. Collins and D.E. Soper, *Nucl. Phys.* **B194** (1982) 445.

[3] I.I. Balitskii and V.M. Braun, *Nucl. Phys.* **B311** (1989) 541.

[4] K.G. Wilson, *Phys. Rev.* **179** (1969) 1499.

[5] L. Mankiewicz and Z. Ryzak, *Phys. Rev.* **D43** (1991) 733.

[6] R.L. Jaffe and A. Manohar, *Nucl. Phys.* **B337** (1990) 509.

[7] X. Ji, private communication.

[8] B.L. Ioffe, *Phys. Lett.* **B30** (1969) 123.

[9] V. Del Duca, S.J. Brodsky and P. Hoyer, *Phys. Rev.* **D46** (1992) 931.

[10] V. Braun, P. Gornicki and L. Mankiewicz, *Phys. Rev.* **D51** (1995) 6036.

[11] L. Mankiewicz and T. Weigl, *Phys. Lett.* **B380** (1996) 134.

[12] F. Halzen and A.D. Martin, *Quarks and Leptons: An Introductory Course in Modern Particle Physics* (Wiley, New York, 1984).

[13] X. Ji, J. Tang and P. Hoodbhoy, *Phys. Rev. Lett.* **76** (1996) 740.

[14] R.L. Jaffe, *Phys. Lett.* **B365** (1996) 359.

[15] L. Mankiewicz, *Phys. Rev.* **D43** (1991) 64, and references therein.

[16] M. Anselmino, A. Efremov, and E. Leader, *Phys. Rep.* **261** (1995) 1.

[17] X. Ji and J. Tang, *Phys. Lett.* **B362** (1995) 182.

[18] S.J. Brodsky and B. Ma, *Phys. Lett.* **B381** (1996) 317.

[19] X. Artru and M. Mekhfi, *Z. Phys.* **C45** (1990) 669; *Nucl. Phys.* **A532** (1991) 351c.

[20] R.L. Jaffe, *Phys. Rev.* **D54** (1996) 6581.

[21] J. Ellis, D. Kharzeev, and A. Kotzinian, *Z. Phys.* **C69** (1996) 467.

[22] J.C. Collins, *Nucl. Phys.* **B396** (1993) 161; J.C. Collins *et al.*, *Nucl. Phys.* **B420** (1994) 565.

[23] P.J. Mulders and R.D. Tangerman, *Nucl. Phys.* **B461** (1996) 197; Erratum ibid. **B484** (1997) 538.

[24] A.V. Efremov, L. Mankiewicz and N.A. Tornqvist, *Phys. Lett.* **B284** (1992) 394.

[25] M. Düren, *Longitudinal Electron Polarization at HERA and the Status of HERMES*, Proc. of the 27^{th} Int. Conf. on HEP, Glasgow, 1994.

[26] D.P. Barber *et al.*, *Phys. Lett.* **B343** (1995) 436.

[27] A.A. Sokolov and I.M. Ternov, *Sov. Phys. Doklady* **8** (1964) 1203.

[28] D.P. Barber *et al.*, *Nucl. Instr. Meth.* **A329** (1993) 79.

[29] K. Lee *et al.*, *Nucl. Instr. Meth.* **A333** (1993) 294.

[30] F. Stock *et al.*, *Nucl. Instr. Meth.* **A343** (1994) 334.

[31] K.P. Coulter *et al.*, *Phys. Rev. Lett.* **68** (1992) 174.

[32] EHS-NA22 Collaboration (M. Adamus *et al.*), *Z. Phys.* **C39** (1988) 311-329.

[33] H1 Collaboration (S. Aid *et al.*), *Phys. Lett.* **B358** (1995) 412-422, DESY-95-156 (August, 1995).

[34] W.R. Frazer *et al.*, *Rev. Mod. Phys.* **44** (1972) 284; J.D. Bjorken and J.B. Kogut, *Phys. Rev.* **D8** (1973) 1341.

[35] T. Sjostrand, *Int. J. Mod. Phys.* **A3** (1988) 751.

[36] B.R. Webber, "Hadronization", lecture given at Summer School on Hadronic Aspects of Collider Physics (Zuoz, Switzerland, 23-31 Aug., 1994).

[37] Ya.I. Azimov, Yu.L. Dokshitser, V.A. Khoze, and S.I. Troian, *Phys. Lett.* **B165** (1985) 147-150.

[38] Ya.I. Azimov, Yu.L. Dokshitser, V.A. Khoze, and S.I. Troian, *Z. Phys.* **C27** (1985) 65.

[39] ARGUS Collaboration (H. Albrecht *et al.*), DESY-96-015 (January, 1996).

[40] H1 Collaboration (S. Aid *et al.*), *Nucl. Phys.* **B445** (1995) 3-24, DESY-95-072 (April, 1995).

[41] E.L. Berger, "Semi-Inclusive Inelastic Electron Scattering from Nuclei", ANL-HEP-CP-87-45 (30 April, 1987).

[42] J. Siegrist *et al.*, *Phys. Rev.* **D26** (1982) 969.

[43] E.L. Berger, *Nucl. Phys.* **B85** (1975) 61.

[44] TASSO Collaboration (M. Althoff *et al.*), *Z. Phys.* **C29** (1985) 347-359.

[45] EHS-NA22 Collaboration (V.V. Aivazyan *et al.*), *Z. Phys.* **C51** (1991) 167-178.

[46] European Muon Collaboration (M. Arneodo *et al.*) *Z. Phys.* **C31** (1986) 333.

[47] European Muon Collaboration (M. Arneodo *et al.*), *Z. Phys.* **C40** (1988) 347.

[48] European Muon Collaboration (M. Arneodo *et al.*), *Z. Phys.* **C31** (1986) 1.

[49] L. Mankiewicz, A. Schäfer and M. Veltri, *Comp. Phys. Comm.* **71** (1992) 305; H. Ihssen, private communication.

[50] D. Graudenz, *Nucl. Phys.* **B432** (1994) 351.

[51] L. Trentadue and G. Veneziano, *Phys. Lett.* **B323** (1994) 201.

[52] European Muon Collaboration (M. Arneodo *et al.*), *Phys. Lett.* **165B** (1985) 222.

[53] N. Pavel, *Nucl. Phys.* **A532** (1991) 465.

[54] T. Gehrmann and W.J. Stirling, *Phys. Rev.* **D53** (1996) 6100, set Gluon A (LO).

[55] R.L. Jaffe and X. Ji, *Nucl. Phys.* **B375** (1992) 527.

[56] D.L. Adams *et al.*, *Phys. Lett.* **B264** (1991) 462.

[57] C. Boros, Z. Liang, and T. Meng, FUB-HEP-95-21-REV (March, 1996), **hep-ph/9603236**.

[58] J. Ralston and D.E. Soper, *Nucl. Phys.* **B154** (1979) 109.

[59] R.L. Jaffe and X. Ji, *Phys. Rev. Lett.* **67** (1991) 552.

[60] X. Ji, *Phys. Rev.* **D52** (1995) 2960.

[61] G. Altarelli and G.G. Ross, *Phys. Lett.* **B212** (1988) 391.

[62] R.D. Carlitz, J.C. Collins and A.H. Mueller, *Phys. Lett.* **B214** (1988) 229.

[63] G. Altarelli and W.J. Stirling, *Part. World* **1** (1989) 40.

[64] S. Forte, *Phys. Lett.* **B224** (1989) 189; *Nucl. Phys.* **B331** (1990) 1.

[65] A. Manohar, *Phys. Rev. Lett.* **65** (1990) 2511.

[66] G.T. Bodwin and J. Qui, *Phys. Rev.* **D41** (1990) 2755.

[67] L. Mankiewicz and A. Schäfer, *Phys. Lett.* **B242** (1990) 455.

[68] S.D. Bass and A.W. Thomas, *Phys. Lett.* **B312** (1993) 345.

[69] S. Gülenstern *et al.*, *Phys. Lett.* **B312** (1993) 166.

[70] S.D. Bass, *Phys. Lett.* **B367** (1996) 335.

[71] L. Mankiewicz, G. Piller and A. Saalfeld, *Phys. Lett.* **B395** (1997) 318.

[72] G. Altarelli and B. Lampe, *Z. Phys.* **C47** (1990) 315.

[73] R.L. Jaffe and X. Ji, *Phys. Rev. Lett.* **71** (1993) 2547.

[74] RHIC Spin Collaboration: Letter of Intent, RHIC-SPIN-LOI-1991 (May, 1991).

[75] A.M. Smith *et al.*, *Phys. Lett.* **185B** (1987) 209.

[76] B. Lundberg *et al.*, *Phys. Rev.* **D40** (1989) 3557.

[77] E.J. Ramberg *et al.*, *Phys. Lett* **338B** (1994) 403.

[78] X. Ji and Z-K Zhu, MIT-CTP-2259 (1993), **hep-ph/9402303** (Submitted to *Phys. Rev. Lett.*).

[79] European Muon Collaboration (M. Arneodo *et al.*), *Nucl. Phys.* **B321** (1989) 541; EMC (J. Aubert *et al.*), *Phys. Lett.* **B160** (1985) 417.

[80] E143 Collaboration (K. Abe *et al.*), *Phys. Rev. Lett.* **76** (1996) 587.

[81] S. Wandzura and F. Wilczek, *Phys. Lett.* **B72** (1977) 195.

[82] M. Düren, *The HERMES Experiment: From the Design to the First Results*, DESY HERMES-95-02 (July, 1995).

[83] J. Bartelski and S. Tatur, *Z. Phys.* **C71** (1996) 595.